RSC Advances

REVIEW

View Article Online
View Journal | View Issue

Cite this: *RSC Adv.*, 2021, **11**, 15301

Sodium silicate-derived aerogels: effect of processing parameters on their applications

Minju N.,[abc] Balagopal N. Nair[de] and Savithri S.*[abc]

Inorganic silica aerogels derived from sodium silicate are voluminous three-dimensional open networks with exceptional properties such as a density as low as ~100 kg m^{-3}, high porosity (~99%), low thermal conductivity (~0.01 W m^{-1} K^{-1}), high specific surface area (~1000 m^2 g^{-1}), low refractive index (~1.05) and high optical transmittance (~95%) depending on their preparation conditions. They are processed through the sol–gel route, which is a reliable methodology to produce high-grade porous materials. Ambient pressure drying has been developed as a low-cost route for the preparation of sodium silicate-derived aerogels, overcoming the difficulties with the use of organosilane precursors and super critical drying. Silica aerogels can be hydrophobic or hydrophilic depending on their synthetic procedure and surface silanol groups. Owing to their unusual properties, these inorganic aerogels have been applied in both commercial and high-tech engineering applications such as thermal insulation, separation, coatings, optics, nuclear particle detection, sensing, and catalysis. This review provides information on the unique features of a wide array of silica aerogels and their potential applications and recent developments in the field of science and technology.

Received 18th November 2020
Accepted 27th March 2021

DOI: 10.1039/d0ra09793d

rsc.li/rsc-advances

1. Introduction

Sodium silicate $(Na_2SiO_2)_nO$ is a fluid substance made by melting sand and excess alkali, which was first observed by chemist van Helmont in 1640. A well-known member of the series is sodium metasilicate, which is known as liquid glass, water glass and soluble glass. These compounds are glassy, colorless and soluble in water, which enhances their functional

[a]*Material Science and Technology Division, CSIR-National Institute for Interdisciplinary Science and Technology, Government of India, Thiruvananthapuram, Kerala 695019, India*

[b]*Computational Modeling and Simulation Section, Environmental Technology Division, CSIR-National Institute for Interdisciplinary Science and Technology, Government of India, Thiruvananthapuram, Kerala 695019, India. E-mail: sivakumarsavi@gmail.com*

[c]*Academy of Scientific and Innovative Research, Ghaziabad, Uttar Pradesh 201002, India*

[d]*R&D Centre, Noritake Company Ltd, 300 Higashiyama, Miyoshi, Aichi 470-0293, Japan*

[e]*School of Molecular and Life Sciences, Faculty of Science and Engineering, Curtin University, GPO Box U1987, Perth, Western Australia 6845, Australia*

Minju N. is a final year PhD scholar at the Materials Science and Technology Division at CSIR-NIIST Trivandrum, India. She completed her Master of Technology in Computer Aided Process Design in 2013 and Bachelor of Technology in Chemical Engineering in 2011 from the Government Engineering College Kozhikode under the University of Calicut. She has five publications in international journals and has attended five conferences with a best oral presentation award to her credit. Her current research is focused on silica porous materials and their sorption applications, and CFD modeling and simulation studies.

Balagopal Nair received his Doctor of Engineering from the Department of Chemical System Engineering, University of Tokyo, Japan and MBA from the Graduate School of International Corporate Strategy, Hitotsubashi University, Tokyo, Japan. Currently, he is employed as a Research Manager at the R&D Center of Noritake Company Ltd Aichi, Japan. Dr Nair is a Fellow of the Institute of Engineers, Australia and a Senior Member of the American Institute of Chemical Engineers (AIChE). Much his recent research work focuses on decarbonization and zero-emission technology and product development. He has authored 94 peer-reviewed research papers and holds 37 granted patents.

properties. Due to their potential marketability, this class of compounds has found wide applications in the field of cements, paints, refractories, adhesives, aquaculture, *etc.* Silica porous materials derived from sodium silicate have been used widely as support materials and for high-tech engineering applications.[1,2] Sodium silicate-based composite materials, gels, *etc.* have been well reported since the early 90 s.

For the synthesis of aerogels, sodium silicate has been recognized as a cost-effective silica source, outperforming its counterparts such as expensive alkoxide precursors. However, a major challenge in developing silica aerogels is their fragile nature owing to the presence of sodium ions compared to alkoxide-derived aerogels.[3] Nevertheless, the affordable method of manufacturing and the market for aerogels make this type of material highly desirable. The normal method for the preparation of silica aerogels is the sol–gel process followed by super critical drying/ambient pressure drying. During the sol–gel process, a better understanding of the mutually dependent processing parameters such as the Na_2SiO_3 : H_2O molar ratio, pH of the silica sol, time for aging and washing, solvent exchange process and use of silylating agents can produce good quality aerogels. Specifically, variations in these parameters determine the final properties of the product. Depending on the target application of the synthesized aerogel, a range of variation in the abovementioned parameters is observed. This review presents an in-depth analysis of the use of sodium silicate for the preparation of aerogels, the effect of the processing parameters, and the use of aerogels in different engineering applications. To understand the chemistry of aerogels, one must be knowledgeable about the underlying sol–gel process, which is discussed below.

2. Sol–gel process

The materials derived from the transformation of silica sols to gels and their subsequent drying deliver sol–gel silica porous materials belonging to the classes xerogels and aerogels. These two classes of materials start their journey from sol–gel chemistry, in which the precursors form tiny sol particles that are quite stable, showing the Tyndall effect, and their subsequent cross-linking result in the formation of semi-solid gels. These gels are given special names, which vary depending on the type of liquid that is trapped inside the pores such as 'hydrogel' for water-based gels and 'alcogel' for alcohol (methanol, ethanol, *etc.*)-based gels. A schematic of the routes followed for the sol–gel process as outlined by Brinker and Scherer[4] is given below (Fig. 1).

The sol–gel process is used for the preparation of porous silica bodies whose properties such as pore size distribution, pore volume, surface area depend on the synthetic conditions. Metal alkoxides are popular precursors for gel processing because they react readily with water. Accordingly, numerous publications on the sol–gel synthesis of silica-based porous materials and membranes using alkoxides have been published over the years.[2,5–9] However, the main drawback of alkoxide precursors is their high cost. In addition, most of these materials are highly reactive with water, and therefore only have a very short shelf-life. Furthermore, when inhaled, these alkoxide vapors undergo hydrolysis and are deposited as nanoparticles in the lungs and lining of the nasal membrane. Accordingly, a cheaper alternative to alkoxide precursors is the class of compounds known as water glass. Recently, sodium silicate has emerged from this class of precursors lately and has been exhaustively exploited due to its low cost and abundance. However, the gels formed are more fragile due to the presence of sodium and they require purification before their transformation for specific applications.

The sol–gel process is a two-step reaction, *i.e.*, hydrolysis followed by condensation. In the first step, sodium silicate reacts with water in the presence of an acid to form silicic acid and a sodium salt, followed by polycondensation, delivering a silica gel as the final product. The polycondensation reaction can be assessed by Si nuclear magnetic resonance spectroscopy up to the sol–gel transition point, where the lines increase rapidly in width and become practically unobservable due to the low concentration of Si in the hydrogels. The gelation time is inversely proportional to the rate of gel formation. The mechanism was presented in detail in the study by M-Jose *et al.* in 1997.[10] The effect of hydrophobic groups such as methyl-, dimethyl-, ethyl-, propyl- and phenyl-silanes on the textural properties of silica gels showed that xerogels prepared in the presence of a solvent water–acetone/acrylonitrile system possessed high surface areas and the samples prepared in the presence of water–ethanol/methanol system had increased hydrophobicity at pH 3.5.[11]

The sol to gel transition begins with the formation of fractal aggregates, which grow until they begin to impinge on each other, and near the gel point, bonds form randomly between the nearly stationary clusters.[4] In general, the formation of fractals and their aggregation significantly depend on the pH of the hydrolysis/condensation reaction and the concentration of the reactant solution. Several aggregation models by RLCA (reaction limited cluster aggregation), DLCA (diffusion limited cluster aggregation), *etc.* are possible and are discussed in detail

S. Savithri has been a Chief Scientist at the Materials Science & Technology Division at CSIR-NIIST Trivandrum since 1992. She obtained her Graduate and Post-Graduate Degrees in Applied Mathematics from Maduari Kamaraj University and her PhD in 1992 from IIT Madras. Her research interests include mathematical modelling of solidification & casting processes and CFD simulation of multiphase flows. She has authored 60 publications and has 3 patents. She was a recipient of the IPA award 2015. Dr Savithri is a key member of the team that has commercialized the technical software called FLOW+ for casting design and simulation and has sold 180 licenses in the period 2013–2020.

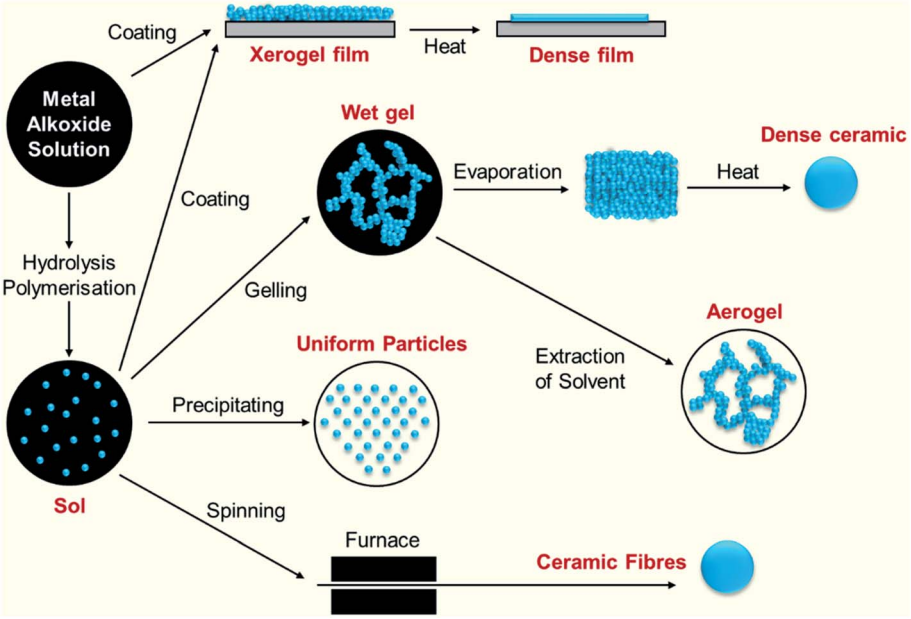

Fig. 1 Schematic route for the sol–gel process.[4]

elsewhere.[4,9,12] Gels of any desired shape can be made by casting the sol in a mold. Even after the gelation point, the bond formation continues, followed by strengthening of the gel network by spontaneous expulsion of the pore liquid and shrinkage of the gel, which is called 'syneresis'. The process of change in the structure and properties after gelation is termed as aging. The unique characteristic of these gels, which cannot be obtained with conventional ceramics, is their porosity. Drying by evaporation under normal conditions gives rise to capillary pressure and shrinkage of the gel network, where the resulting gel, which is called a 'xerogel', usually has 5 to 10 times less volume than the wet gel. Under super critical conditions, there is no capillary pressure and less shrinkage is observed and the product is termed 'aerogel', which is usually ~99% porous.[4]

3. Silica aerogels from sodium silicate

The fascinating discovery of a silica aerogel from sodium silicate by Samuel Kistler occurred in the fall of 1920 during his interest in the research carried by Dr E. L. Alling of Stanford University about the crystallization of amino acids from solution. The accidental discovery of the world's first aerogel was assumed to occur during his investigations on the precipitation of compounds from solution as their critical point approaches. This enigmatic discovery was first documented in Nature publications in 1931.[13] Subsequently, the detailed report was published in the *J. Phys. Chem.*.[14] The first commercial aerogel entered the market in the 1950s under the trade name Santocel, a Monsanto Corp. product. Santocel had an air volume of 94%, thermal conductivity of 0.015 W m^{-1} K^{-1} and bulk density of 0.096 g cc^{-1}. This product found many uses in civilian and military applications such as thermal insulating materials, thickening agents, and ingredient for the manufacture of silicon rubber. This product was followed by other similar products such as Aerosil and Cabosil, which are fumed silica products from silicon tetrachloride. However, there are several drawbacks associated with the commercial production of aerogels. The use of super critical drying (for ethanol $T_c = 516$ K and $P_c = 63$ bar) affects the cost efficiency, continuity and safety of the process due to the high temperature and pressure required to reach the critical point. Even low temperature super critical drying ($T_c = 304$ K and $P_c = 73$ bar) using liquid CO_2 requires considerably high pressures. Furthermore, the condensation of moisture in the hydrophilic network results in a deterioration in insulating properties and capillary stress-induced collapse of the aerogel network.[13] Also, the inability to meet cost/performance indicators compared to other materials used in similar fields has unofficially put an end to the aerogel industry.

The niche area of aerogels was long forgotten until Brinker came up with the ambient pressure drying technique for tetraethylorthosilicate (TEOS)-based aerogels. Specifically, the samples were dried at room temperature for 24 h followed by drying at 323 K for 24 h. The resultant ambient pressure aerogels possessed a BET surface area of 869 m^2 g^{-1}, density of 0.318 g cc^{-1}, large pore volume and striking similarities in morphology to that of super critical aerogels. The structural stability in these materials is due to their hydrophobic nature.[15] Thus, ambient pressure drying emerged as an alternative and attractive method for the commercial production of silica aerogels. Thereafter, several research groups developed silica aerogels from low cost precursors such as sodium silicate,[16–22] where the popular was made by Schwertfeger *et al.* in 1998.[8,23] They prepared silica aerogels by passing sodium silicate through ion exchange resins to replace the Na^+ ions with H^+

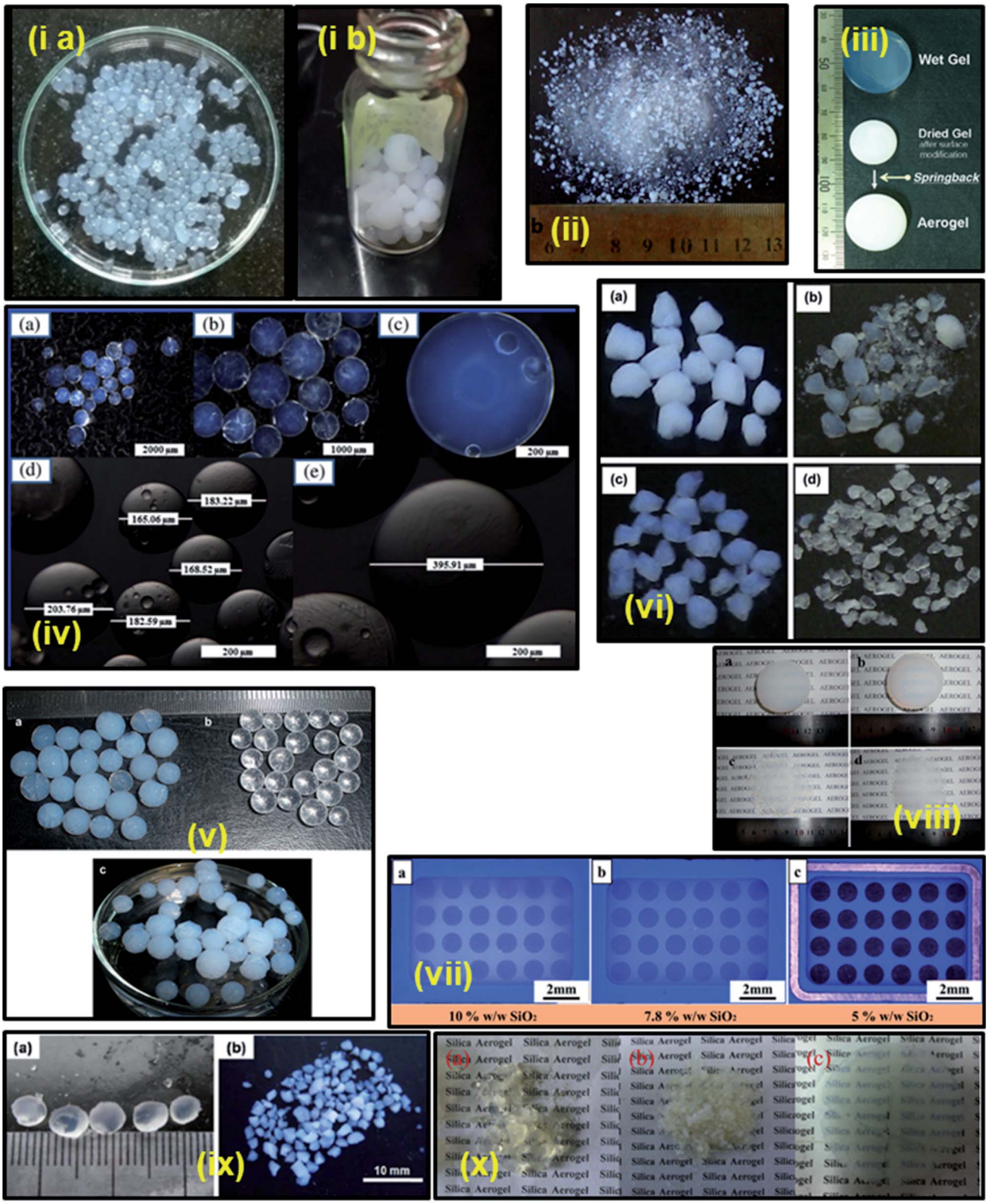

Fig. 2 Different grades of silica aerogels: (i) silica (a) hydrogel and (b) aerogel beads;[39] (ii) ambient pressure dried silica aerogel granules well modified by TMCS;[41] (iii) spring back effect during the ambient drying of surface-modified gel;[20] (iv) transparent micro-silica aerogel beads;[42] (v) (a) TMCS modified (10% V) and (b) unmodified mesoporous silica aerogel beads, and (c) photograph showing the super hydrophobicity of the aerogel beads on the surface of water;[43] (vi) silica aerogels prepared by (a) single step and (b–d) two-step sol–gel process;[44] (vii) aerogel membranes;[7] (viii) mesoporous silica aerogels heat treated at different temperatures (a) untreated, (b) 300 °C, (c) 500 °C, and (d) 800 °C;[45] (ix) (a) silica alcogel spheres and (b) aerogel particles after ambient-pressure drying;[46] and (x) aerogels prepared by (a) co-precursor, (b) surface derivatization and (c) two-step modification.[47]

Table 1 Physical properties of silica aerogels synthesized from sodium silicate by different researchers[a]

Raw material	Solvent used for pore water exchange	Catalyst	Silylating agent	Gelation pH	Drying method	Density (g cm^{-3})	Contact angle (°)	Thermal conductivity (W m^{-1} K^{-1})	Porosity (%)	Pore size (nm)	Surface area (m^2 g^{-1})	Total pore volume (cm^3 g^{-1})	Ref.
Rice husk	EtOH	Sulphuric acid	—	5–5.5	SCD	0.08	—	—	95	11–18	773	3.6	Halim 2018 (ref. 27)
Rice husk ash	EtOH	NaOH	—	5	SCD	0.07	—	—		16.32	729.82	3.39	Sheng 2015 (ref. 30)
Sodium silicate	EtOH	Sulphuric acid	TMCS	6	APD	0.36	—	—	81.7	26.35	719	3.4	Sarawade 2012 (ref. 42)
Sodium silicate	IsoprOH	Acetic acid	—	3.8	APD	—	—	—	—	6.71	473.93	0.02	Minju 2017 (ref. 60)
Industrial grade sodium silicate	Acetone *n*-Hexane	NaOH	Unmodified MPTMS	4–5	APD	—	—	—	—	7.59 3.89	602 387.9	1.15 0.46	Pouretedal 2012 (ref. 61)
Fly ash	EtOH	H_2SO_4	TMCS	10	APD	—	—	—	—	7.69–24.09	362.2–578.5	0.74–3.20	Shi 2010 (ref. 36)
		NaOH		5–6						21.48	907.9	4.88	
Native corn starch	EtOH	Emulsification	TMOS	—	SCD	<0.25	—	—	>85	14–18	1000	—	Garcia 2015 (ref. 62)
Rice husk	EtOH	Acetic acid	TMCS	5	APD	0.07	135	0.041	95	11–20	600–700	2–3	Halim 2018 (ref. 46)
Sodium silicate	EtOH	Acid/base catalysis	—	3.5	APD	0.318	—	—	—	—	869	2.65	Smith 1992 (ref. 15)
Sodium silicate	Hexane	NH_4OH	TMCS	4	APD	—	—	—	—	10	681	—	Sarawade 2006 (ref. 49)
Rice hull ash	EtOH	Nitric acid	TEOS	4–9	APD	0.27–0.85	—	—	61.23–87.53	3.24–10.22	238–673	0.45–1.17	Karakuzu 2016 (ref. 29)
		Citric acid				0.28–0.75			65.71–87.35	3.37–9.43	261–726	0.52–1.06	
Sodium silicate	MeOH	HCl/NH_4F	TMES/TMCS	—	APD	0.14	131.8	—	92.7	14.04	458	3.22	Nah 2018 (ref. 58)
Sodium silicate	MeOH	HCl and NH_4F	TMCS	—	APD	0.1	144.09	—	94.3	27.41	623.2	4.27	Nah 2018 (ref. 40)
Sodium silicate	MeOH	HCl	TMCS	4 8	APD	—	—	—	76.9–89.7 58.2–66.9	14.9–17.4 12.3–25.8	412–485 250–367	2.64–3.65 0.61–1.86	Motahari 2015 (ref. 63)
Sodium silicate/ PMMA	EtOH	NH_4OH	TMCS	5–5.5	APD	0.3–0.78	—	—	45–87	15.62–48.61	256.34–687.28	1.04–3.04	Ma 2016 (ref. 64)
Sodium silicate	*n*-Hexane	Nitric acid	HMDZ	—	APD	0.1–0.5	140–152	—	—	4.78–9.9	394–637	0.45–0.90	Julio 2014 (ref. 57)
Industrial grade sodium silicate	—	H_2SO_4	Unmodified TMCS	5.5	APD	—	—	—	—	8.75 9.49	648.6 487.5	1.48 1.2	Khan 2018 (ref. 39)
Sodium silicate	IsoprOH	NH_4OH	TMCS	—	APD	0.25	146	—	88.6	24	815	3.5 m^3 g^{-1}	Sebdani 2016 (ref. 65)
	IsoprOH	NH_3	TMCS	5	APD	0.18	146.4	—	91.8	23.93	815.14		

Table 1 (*Contd.*)

Raw material	Solvent used for pore water exchange	Catalyst	Silylating agent	Gelation pH	Drying method	Density (g cm^{-3})	Contact angle (°)	Thermal conductivity (W m^{-1} K^{-1})	Porosity (%)	Pore size (nm)	Surface area (m^2 g^{-1})	Total pore volume (cm^3 g^{-1})	Ref.
Sodium silicate												3.53 m^3 g^{-1}	Sebdani 2012 (ref. 66)
Sodium silicate	EtOH	NH_4OH	TMCS	6	APD	0.09–0.17	165	—	92.32–95.34	1.7–50	456–817		He 2015 (ref. 41)
Industrial grade sodium silicate	—	H_2SO_4	—	5	Oven Microwave Spray	0.36 0.29 0.23	—	—	80.95 84.52 88.16	7.51 10.21 17.41	358 437 679	0.91 1.27 1.96	Sarawade 2011 (ref. 67)
Oil shale ash	Hexane	H_2SO_4	HMDZ	7	Fluidized bed drying	0.08	—	—	—	14.1	789	2.77	Gao 2010 (ref. 68)
Industrial grade sodium silicate	EtOH	NH_3	TMCS	—	APD	0.104–0.15	—	0.021–0.031	93.4–95.3	10–12.3	626.2–804.5	2.81–3.45	Shao 2015 (ref. 69)
Sodium silicate	Hexane	HCl	TMCS/HMDSO	10.55,10.85	APD	0.11–0.13	143–145	0.022–0.025	92–93	66–100	310–425	0.40–2.87	Pooter 2018 (ref. 70)
Industrial water glass	EtOH	NH_4OH	TMCS	—	APD	—	—	0.03–0.038	—	10.06–12.15	139–250	0.58–1.06	Jia 2018 (ref. 71)
Water glass	EtOH	HCl	TMCS	6.2	APD	0.09–0.12	106–161	—	91.3–94.5	131–156	469–680	1.8–3.3	He 2015 (ref. 56)
Industrial water glass	EtOH	Oxalic acid	TMCS	4	APD	0.07–0.09	—	—	95.59–96	8.64–16.31	524–776	2.72–3.1	Sarawade 2011 (ref. 72)
Wheat husk ash	EtOH	NH_3	TMCS	5–6	APD	0.06–0.16	147	0.009–0.012	90.1–96.5	9–15	513–587	2.3–4	Liu 2016 (ref. 33)
Rice husk char	—	*ortho*-Phosphoric acid	—	4.9	APD	—	—	—	—	2.07–2.74	709–936	0.37–0.62	Li 2011 (ref. 28)
Water glass	EtOH	NaOH	HMDSO	5.5	APD	0.09–0.11	128, 147	0.022–0.099	91.21–96.33	2–50	466–651	—	Liu 2012 (ref. 45)
Sodium silicate/$TiOCl_2$	EtOH	NH_4OH	TMCS	3.5	APD	0.12–0.47	—	—	—	6.5–14.9	623–726	1.3–3	Kim 2013 (ref. 73)
Sodium silicate	EtOH	NH_4OH	HMDZ	4.6	APD	0.14–0.21	—	—	~82–93	—	—	~2.2–6	Rao 2004 (ref. 48)
Sodium silicate	*n*-Hexane, isoPrOH	Pyridine	TMCS	—	APD	0.12	—	0.01	94	~4–7.5	~560–650	—	Yeo 2007 (ref. 74)
Bamboo leaves	*n*-Hexane	HCl	HMDZ	7	SCD	0.07	—	0.0311	97.9	—	331	1.38	Kow 2016 (ref. 34)
Sodium silicate	MeOH, hexane	Acetic acid	TMCS HMDZ	—	APD	0.04–0.1 0.09–0.12	149 143		95–97.8 93.9–95.1	—	—	10–24.5 16.1–18.7	Shewale 2008 (ref. 16)
Sodium silicate	EtOH, *n*-hexane	NH_3	TMCS	6	APD	0.08			93.6	12.3	917	2.8	Sarawade 2010 (ref. 43)
Sodium silicate	*n*-Hexane/EtOH	H_2SO_4	TMCS	7	Spray drying	0.27	155	—	—	16.4	870	2.2	Sarawade 2010 (ref. 75)
Sodium silicate	MeOH EtOH PrOH	NH_4OH	TMCS	—	APD	0.1 0.16 0.16	166 164 172	0.104 0.115 0.12	94.87 92.05 91.79	120 <100 >130	— — —	9.49 5.94 5.74	Rao 2008 (ref. 21)

Table 1 (*Contd.*)

Raw material	Solvent used for pore water exchange	Catalyst	Silylating agent	Gelation pH	Drying method	Density (g cm^{-3})	Contact angle (°)	Thermal conductivity (W m^{-1} K^{-1})	Porosity (%)	Pore size (nm)	Surface area (m^2 g^{-1})	Total pore volume (cm^3 g^{-1})	Ref.
	IsoPrOH					0.07	166	0.091	96.6	>130	—	13.77	
	BuOH					0.17	163	0.13	91.28	<100	—	5.37	
	IsoBuOH					0.17	161	0.122	91.54	>130	—	5.55	
	Hexanol					0.19	165	0.21	90.03	—	—	4.75	
Sodium silicate	MeOH/*n*-hexane	NH_4F/HCl	TMCS	—	APD	0.13	143	0.128	93.4	17.9	425	2.29	Bangi 2013 (ref. 44)
Fly ash acid sludge	EtOH	NH_4OH	TMCS	5–6	APD	0.09	140	—	—	12.62	700	3.29	Cheng 2016 (ref. 37)
Sodium silicate	*n*-Hexane	HNO_3	HMDS	—	FBD	0.05–0.07	—	—	—	8.5–8.75	639–783	1.43–1.79	Bhagat 2008 (ref. 17)
Sodium silicate	*n*-Hexane	HNO_3	HMDS	—	APD	0.08–0.64	150	—	—	5.4–10.1	173–778	0.25–2.34	Bhagat 2008 (ref. 18)
Sodium silicate	MeOH	Tartaric acid	TMCS	—	APD	0.08	146	0.09	95	—	—	11.4	Bangi 2008 (ref. 19)
Rice hull ash	EtOH	H_2SO_4	TEOS	—	APD	0.33	—	—	87	26.5	499	3.31	Li 2008 (ref. 25)
Sodium silicate	IsoPrOH	NH_3	TMCS	5	APD	0.13–0.16	—	—	80.8–83.8	6–16	677.94–1046.88	—	Kim 2007 (ref. 76)
Rice husk ash	EtOH	HNO_3	TEOS	6	APD	0.67	—	—	80	10–40	273	3.1	Nayak 2009 (ref. 26)
Sodium silicate	EtOH	NH_4OH	TMCS	—	APD	0.1–0.3	—	—	88–96	10	730–950	—	Lee 2006 (ref. 55)
Sodium silicate	MeOH	Tartaric acid	TMCS	—	APD	0.07	145	—	97	70	510	14.62	Gurav 2009 (ref. 52)
Sodium silicate	EtOH	NH_3/H_2SO_4	TEOS	—	APD	0.14	—	—	93.7	9.72	610.64	1.48	Geng 2010 (ref. 50)
Industrial grade sodium silicate	*n*-Hexane	NH_4OH	TMCS	3.5	APD	0.12–0.14	≥ 120		92–95	9.7–11.04	670–724	3.36–3.48	Hwang 2008 (ref. 20)
Water glass	—	NaOH	HMDSO/TMCS	—	N_2 steam of 1500 L h^{-1} at 200 °C	0.1 0.16	—	0.01–0.015	>85	14	700	92	Schwertfeger 1998 (ref. 23)
Sodium silicate	EtOH	NH_4OH	HMDZ	5–6	SCD	0.07–0.13	123–149	0.015–0.017	94–97	36.9–142	441–782	7.2–15.7	Zhao 2015 (ref. 7)
Rice husk ash	EtOH	H_2SO_4	TEOS	—	APD	0.32	—	—	85	9.8	315	0.78	Tadjarodi 2012 (ref. 31)
Industrial micro silica	EtOH	NaOH	TMCS	6	APD	0.11–0.19	130	—	91.5–95.1	5.22–8.02	767–828	1.61–2.78	Shi 2013 (ref. 77)
Sodium silicate	*n*-Hexane	HNO_3	HMDS/TMCS/TEOS	—	APD	—	103–109	—	—	17.1–17.78	345–936	0.395–1.715	Sorour 2016 (ref. 78)
Bagasse ash	—	NH_4OH	TMCS/HMDS	8–9	APD	—	—	—	—	5.7–12.3	450.2–1360.4	0.75–1.93	Nazriati 2011 (ref. 79)

Table 1 (*Contd.*)

Raw material	Solvent used for pore water exchange	Catalyst	Silylating agent	Gelation pH	Drying method	Density (g cm^{-3})	Contact angle (°)	Thermal conductivity (W m^{-1} K^{-1})	Porosity (%)	Pore size (nm)	Surface area (m^2 g^{-1})	Total pore volume (cm^3 g^{-1})	Ref.
Sodium silicate	EtOH	NH_3	MTES/TMCS	—	APD	0.12–0.61	80–146	—	72.3–94.5	3.34–14.28	665.73–971.23	0.71–3.55	Shao 2013 (ref. 47)
Sodium silicate	Hexane	NH_3	TMCS	4–5	APD	0.18	145	—	—	17.67	823	3.63	Yaqubzadeh 2016 (ref. 80)
Water glass	EtOH	CO_2 gas	MTMS/TMCS	9	APD	—	154	—	—	33–71.4	314–492	0.0733–0.1595	Wu 2018 (ref. 81)
Rice husk ash	EtOH	Acetic acid	TEOS	7	APD	0.37	—	—	83	10.7	294.4	1.022	Temel 2017
		HCl				0.38			83	11.79	268	0.998	(ref. 32)
		HNO_3				0.29			87	11.19	287.7	0.923	
		Oxalic acid				0.21			90	10.85	322.5	1.048	
		H_2SO_4				0.39			82	10.33	294.9	1.044	
Sodium silicate	MeOH	Citric acid	DMCS	—	APD	0.23	140	0.125	87.8	—	—	—	Rao 2011 (ref. 82)
			DMDC			0.22	142	0.122	88.2				
			TMCS			0.09	144	0.091	95.7				
			HMDZ			0.22	140	0.122	88.3				
			HMDSO			0.52	< 90	0.19	72.8				
Bagasse ash	—	NH_4OH	TMCS/HMDS	4	APD	—	140	—	—	3.77	1113.76	2.13	Nazriati 2014 (ref. 35)
Water glass	EtOH	HCl/diluted water glass	TMCS	5	APD	0.0762	162.3	0.0237	96.54	13.8	776.1	3	Pan 2017 (ref. 83)
Sodium silicate	EtOH	NH_4OH	MTMS	—	APD	0.152	60	0.164	92.05	—	—	6.05	Rao 2007 (ref. 54)
			MTES			0.164	65	0.170	91.45			5.51	
			VTMS			0.157	70	0.169	91.94			5.84	
			PTMS			0.145	80	0.154	92.56			6.37	
			PTES			0.149	85	0.152	92.15			6.18	
			DMDMS			0.131	88	0.134	93.32			7.10	
			TMMS			0.110	130	0.121	94.35			8.58	
			TMCS			0.105	155	0.118	94.61			9.01	
			BTSA			0.090	150	0.102	95.38			10.60	
			HMDZ			0.060	165	0.091	96.90			16.15	
Recycled coal gangue	Heptane/EtOH	H_2SO_4	TMCS	—	APD	0.19	—	0.027	91.4	27.5	690	4.81	Zhu 2016 (ref. 84)
Sodium silicate	MeOH	NH_4F/HCl	TMCS	—	APD	0.11	142	0.12	—	—	560	—	Bangi 2019 (ref. 85)
Sodium silicate	MeOH	Citric acid monohydrate	FAS	—	SCD	—	145–158	—	—	2.6–3.4	280.1–590.2	0.18–0.53	Lin 2019 (ref. 86)

[a] APD – ambient pressure drying, SCD – super critical drying, FBD – fluidized bed drying, EtOH – ethanol, MeOH – methanol, PrOH – propanol, IsoPrOH – isopropanol, BuOH – butanol, IsoBuOH – isobutanol, TMCS – trimethylchlorosilane, MPTMS – mercaptopropyl trimethoxysilane, TMOS – tetramethoxysilane, TEOS – tetraethoxysilane, TMES – trimethylethoxysilane, HMDZ/HMDS – hexamethyldisilazane, HMDSO – hexamethyldisiloxane, MTES – methyltriethoxysilane, MTMS – methyltrimethoxysilane, MTES – methyltriethoxysilane, DMCS – dimethylchlorosilane, DMDC – dimethyldichlorosilane, VTMS – vinyltrimethoxysilane, PTMS – phenyl trimethoxysilane, PTES – phenyl triethoxysilane, DMDMS – dimethyldimethoxysilane, TMMS – trimethylmethoxysilane, BTSA – bis(trimethylsilyl) acetamide, HMDZ – hexamethyldisilazane, and FAS – fluoroalkylsilane.

ions, followed by a sol–gel transition and ambient pressure drying. Silicic acid with high purity can be obtained by passing sodium silicate through ion exchange resin.[24] However, the use of ion exchange resin is a costly and time-consuming process. Aerogels were also prepared without prior ion exchange to produce silica aerogel powders *via* fluidized bed drying, possessing properties such as a tapping density value as low as 0.05 g cc^{-1}, high specific surface area of 783 m^2 g^{-1} and cumulative pore volume of 1.79 cm^3 g^{-1}.[17] The hydrolysis and condensation occurred according to reactions (1) and (2) as follows:[16]

Hydrolysis:

$$Na_2SiO_3 + H_2O + 2CH_3COOH \rightarrow Si{-}(OH)_4 + 2CH_3COONa \quad (1)$$

Condensation:

$$Si{-}(OH)_4 + (HO)_4{-}Si \rightarrow (HO)_3{-}Si{-}O{-}Si{-}(OH)_3 + H_2O \quad (2)$$

Initially, sodium silicate was dissolved in distilled water and a homogenous sol was prepared *via* the dropwise addition of acidified water to form silicic acid and a sodium salt. This is the initial hydrolysis stage in which Si–OH bonds are formed. Subsequently, a condensation step occurs *via* the expulsion of water to form a highly cross-linked gel network called a 'hydrogel' in which water is entrapped in the porous network. These hydrogels are highly sensitive to the outside atmospheric conditions, and hence proper aging is required to strengthen the gel network. The presence of sodium ions will induce brittleness in the gel. Thus, to tackle this issue, the aged gel is washed several times with a surplus amount of water to remove the Na^+ ions. Then the water in the pores is replaced with any suitable organic solvent to form alcogels. Surface functionalization with different silanes induces hydrophobicity and helps to minimize the surface tension and prevent cracking of the final product.[16–21] Sodium silicate extracted from biomaterials such as rice husk,[25–29] rice husk ash,[30–32] wheat husk ash,[33] bamboo leaves,[34] bagasse ash,[35] fly ash,[36] and fly ash acid sludge[37,38] have also been used for the synthesis of aerogels. In these cases, silica is extracted from the precursors as sodium silicate by boiling in NaOH solution. Aerogels with a density of 0.33 g cm^{-3} and surface area of 648 m^2 g^{-1} can be prepared from ash through this method.[25] Industrial grade sodium silicate can also produce aerogels having a surface area of around 649 m^2 g^{-1} (Fig. 2(i)).[39] Oxalic acid has also been used as a drying control chemical additive to improve the physical properties of sodium silicate aerogels. Aerogels with a molar ratio of 15×10^{-4} oxalic acid to Na_2SiO_3 showed enhanced properties such as high porosity of 94.3%, high specific surface area of 623.2 m^2 g^{-1}, low density of 0.1 g cm^{-3} and high optical transmittance of 75%.[40] Fig. 2 shows various grades of silica aerogels synthesized under different operating conditions and modifications.

4. Key parameters for the preparation of gels

Different parameters such as the molar ratio of Na_2SiO_3 to H_2O, pH of the medium, drying method and conditions have a considerable effect on the physical properties of the final gel product, each of which are described in detail below. The silica aerogels synthesized by different researchers and their physical properties are presented in detail in Table I.

4.1 Na_2SiO_3 : H_2O molar ratio

The Na_2SiO_3 : H_2O molar ratio, which reflects the silica content present in the gels, is an important factor in the preparation of sodium silicate gels. As the molar ratio increases, the SiO_2 content in the sample increases, thereby generating a strong network of Si–O–Si bonds. Owing to the larger syneresis effect in these gels, rapid expulsion of the pore liquid occurs. This marks

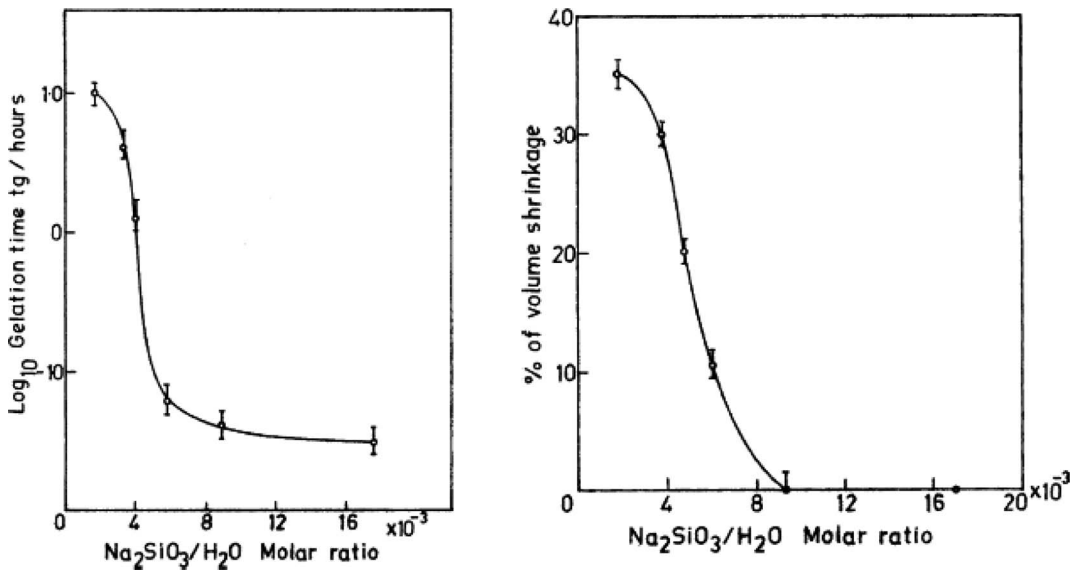

Fig. 3 Graph showing the variation in gelation time and volume shrinkage with Na_2SiO_3/H_2O molar ratio.[48]

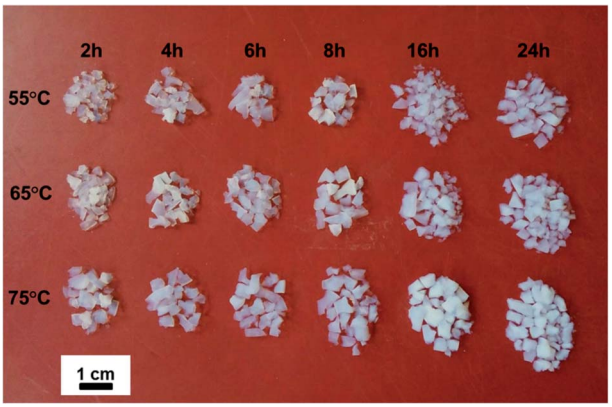

Fig. 4 Silica aerogels dried at ambient pressure for different aging times and at different temperatures.[53]

in a decrease in the gelation time and bulk density of the aerogels. In the study done by Rao *et al.* in 2004,[48] for a molar ratio $> 8.86 \times 10^{-3}$, no shrinkage of the gel network was observed. When the molar ratio decreased, the gelation time became considerably slow, and an excess number of hydroxyl groups resulted in the formation of a sol, which hindered the cross-linking of the siloxane networks (Fig. 3). Diluting the sodium silicate with too much water will result in loose linkages, causing poor mechanical strength and collapse of the gel during ambient pressure drying (Fig. 2(ii)).[41] When the SiO_2 content increased, the bulk modulus of the gel was high and less shrinkage occurred, and consequently the density was lower. However, with an increase in pore size, the optical transmission decreased. The maximum optical transmission was observed for a molar ratio of less than 4×10^{-3}.[48] The percentage porosity and pore volume of the gel increased with an increase in the molar ratio of $Na_2SiO_3 : H_2O$.

4.2 Effect of sol pH

The gels formed from water glass can either be acidic or basic gels depending on the methods used to initiate the gelation process. The two common ways include the addition of a Bronsted acid for partial neutralization of the sodium silicate solution or the use of ion-exchange resin to replace the Na^+ ions with H^+ ions, forming a silicic acid solution and initiating gelation by the addition of a Lewis base or Bronsted base. The gels form faster at intermediate pH values.[9]

When the pH is >4, the gelation time and density of the gel decrease, whereas the porosity of the aerogel increases above 95%. When the pH is <4, a higher gelation time and density and lower porosity (<90%) prevail. At pH <4, the sodium silicate solution exists in the silicic acid form, *meta*-silicic acid H_2SiO_3 and *ortho*-silicic acid H_4SiO_4. The small silicic acid oligomers undergo stepwise condensation to produce a large number of Si–O–Si linkages. The gelation time is longer and the chance of the silica particles fusing is much less. From pH 3 to 8, the gels range from transparent and semi-transparent to opaque. A saturated water glass solution has a density in the range of 1.4 g cm^{-3} and pH ~13. At pH >10, sodium silicate is the dominant species, and hence the condensation reaction will be slow, resulting in competition between the forward and backward reactions. Thus, water glass solutions do not gel at high pH.[9] In the work done by Sarawade *et al.* in 2006, the 'gel point' is defined at around pH 5, at which the silica monomer begins to form a gel network and the viscosity of the sol increases and gelation occurs.[49,50] Here, the gelation time is minimum and the surface is partly occupied by $Si–O^-$ groups. At this point, the aggregation is diffusion limited.[51] Thus, in conclusion, the condensation and gelation of silica preferably occur in the pH range of 5–9.[9]

4.3 Effect of aging, washing and solvent exchange

The aging of the gel after synthesis helps to strengthen the silane network, thereby reducing the chance of the gel cracking. With an increase in the aging time, the density of the gel decreases to a critical point, beyond which the density increases. A freshly formed gel is very fragile and sensitive to the external atmosphere. Even after gelation, polycondensation continues and aging of the gel causes thickening of the network owing to the dissolution and reprecipitation of the silica oligomers. Thus, only minimum shrinkage occurs, resulting in low density aerogels. When the aging time increases beyond 1 h, more connecting bonds are formed and the network contracts again, which leads to shrinkage of the gels together with the syneresis of the liquid, Ostwald ripening, and segregation,[48] and hence an increase in density.[52] Iswar *et al.* in 2016 observed that the aging of gels within the gelation liquid without any solvent exchange could produce low density silica aerogels by ambient pressure drying and post treatments with strengthening agents such as TEOS/TMOS. With an increase in aging time and temperature, the bulk density and surface area of the aerogel decrease (Fig. 4).[53]

The washing of the gel after aging is a crucial step to eliminate the Na^+ ions from the system. When sodium ions are present, they induce brittleness in the gel and subsequent cracking. The greater the extent of washing, the lower the content of Na^+. Gurav *et al.* used water vapour to remove the Na^+ ions from the system by passing the vapors through a hydrogel.

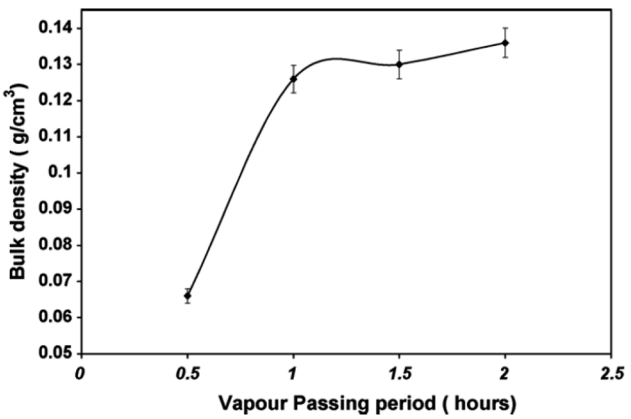

Fig. 5 Graph showing the change in density with the water vapour passing period and gel aging period.[52]

Table 2 Characteristic FTIR peaks of silica aerogels[47,54,55]

Peak positions	Chemical bonds
Strong absorption peak near 1090 cm^{-1}, 1180 cm^{-1} and weak peak at around 800 cm^{-1}	Asymmetric and symmetric bending of Si–O–Si
Strong peak near 460 cm^{-1}	Bending of O–Si–O
Weak peak at around 2950 cm^{-1} and 2900 cm^{-1}	CH_3 terminal from surface treatment
Peaks near 1276, 1260, 867, 850 and 758 cm^{-1}	Si–C originating from surface treatment
Wide band at around 3500 cm^{-1} and the peak at around 1600 cm^{-1}	Surface-adsorbed hydroxyl groups
Oscillations between 1300 cm^{-1} and 1650 cm^{-1}	Bending of H–O–H
Weak peak near 960 cm^{-1}	Stretching of Si–OH
Peaks at 2980, 2926, and 1450 cm^{-1}	CH_3 and CH_2 bonds

For the gels prepared with the $Na_2SiO_3 : H_2O : C_4H_6O_6$ molar ratio of 1 : 166.6 : 2.5, with an increase in the vapour passing period from 0.5 to 2 h, the bulk density increased from 0.066 to 0.136 g cm^{-3}. As the pressure exerted by the vapour increases, the stress on the gel increases. Hence, shrinkage occurs until the bulk modulus of the gel network increases up to certain limit to resist the applied vapour pressure (Fig. 5).[52]

The water flows through the gel according to Darcy's law, as shown by eqn (3),

$$J = \left(\frac{D}{\eta_L}\right)\nabla P \quad (3)$$

where η_L is the viscosity of the liquid, D is the gel permeability and ∇P is the pressure gradient.[52]

For the solvent exchange process, alcohols are considered as the ideal choice, where during the change over from the protic to aprotic phase, due to the bifunctional nature of alcohols, they promote the miscibility between the aqueous and organic phase. The physical properties of the final material depend considerably on the type of solvent chosen, as shown in Table I. In the work by Rao *et al.* in 2008,[21] solvents with lower vapor pressure and low surface tension produced low density aerogels. When the surface tension is low, the capillary pressure exerted will be lower. The capillary pressure depends on the surface tension of the pore liquid, 'γ_{LV}', pore radius, 'r_p', and thickness of the surface adsorbed layer, 't', as given eqn (4):[4]

$$P_c = -\frac{2\gamma_{LV}}{(r_p - t)} \quad (4)$$

4.4 Effect of silylating agents

To make the whole synthesis procedure economical, it is important to identify the minimum amount of silylating agents needed per SiO_2. In a study done using the surface modification agent HMDS, at an HMDS : Na_2SiO_3 molar ratio of less than 4, the density of the gel decreased from 0.117 to 0.095 g cm^{-3}. With an excess molar ratio, the density increased beyond 0.2 g cm^{-3} and the optical transmittance decreased to less than 20%. This is due to the increase in steric hindrance, which leads to structural collapse and opacity of the aerogel.[16] The physical properties of the hydrophobic aerogels synthesized with different silylating agents were documented by Rao *et al.* in 2007 (Table I).[54]

The properties of the aerogels synthesized are listed in Table II below. Extensive research has been conducted on different mono(methyltrimethoxysilane) (MTMS), methyltriethoxysilane (MTES),[47] vinyltrimethoxysilane (VTMS), phenyl trimethoxysilane (PTMS), phenyl triethoxysilane (PTES)), di(dimethyldimethoxysilane) (DMDMS), tri(trimethylmethoxysilane) (TMMS), trimethylchlorosilane (TMCS),[20,33,35,37,39,41,55,56] bis(trimethylsilyl) acetamide (BTSA), hexamethyldisilazane (HMDZ),[57] and hexamethyldisiloxane (HMDSO)[20,45] alkyl silylating agents by various research groups.[54] To avoid the use of TMCS, which forms HCl after silylation, trimethyl ethoxy silane (TMES) was explored instead. The physical properties of the aerogel were improved on surface modification with a combination of TMCS and TMES compared to the unmodified aerogel.[58] The mixing time of the silylating agents with the silica precursors reportedly influenced the surface area of the silica aerogels.[35]

With an increase in the silylation period, the aerogel density and thermal conductivity decreased, whereas the porosity and hydrophobicity increased.[19] With an increase in the alkyl groups in the silylating agents, the density of the aerogels decreased, and the pore volume and % porosity increased. This can be explained based on the attachment of the Si–R groups on the surface of the silica, resulting in a hydrophobic surface.

The surface modification reaction is given as eqn (5):

$$\underset{\text{silica gel}}{4 - n(\equiv Si - OH)} + \underset{\text{silylating agent}}{(RO)_{4-n}SiR_n} \rightarrow \underset{\text{surface modified silica gel}}{(\equiv Si - O)_{4-n}Si - R_n} + \underset{\text{alcohol}}{(4 - n)ROH} \quad (5)$$

For unsilylated hydrophilic silica aerogels, the surface –OH groups start condensing, while drying leads to a shrinkage in the volume of the gels. The shrinkage happens until all the pore liquid has been evaporated, giving the final volume of the gel. The key factor determining shrinkage is the capillary pressure of the pore liquid. For cylindrical pores, the magnitude of the capillary pressure of the pore fluid is governed by eqn (6):

$$P_c = -2\gamma \cos\theta / r_c \quad (6)$$

where P_c is the capillary pressure, γ is the surface tension, r_c is the characteristic capillary rise equivalent to pore size, r_p. For a wetting liquid (<90°), the magnitude is negative, indicating

that the liquid is in tension. Thus, the wet gel is washed with solvents or mixtures of solvents having different surface tensions to yield the desired shrinkage and the contact angle of most solvents appear to be ~0°.[54,59]

In case of silylated aerogels, the surface is modified to O–Si–$(CH_3)_3$. Here the % decrease in volume will be due to the expulsion of the pore liquid only. Also, when the drying temperature is increased, the CH_3 groups come closer, and a repulsive force occurs between each hydrophobic group, leading to a 'spring back' effect to the original volume (Fig. 2(iii)). The greater the intensity and surface modification with silylating agents, the lower the density and greater the porosity, as seen in Table I. The intensity in the surface modification decreases in the order of tri > di > mono alkyl silanes. For mono alkyl silanes, when the alkyl group is bulkier, the spring back effect is greater, and therefore the resulting gel is less dense. Therefore, the density of PTMS will be less compared to MTMS. The greater the spring back effect, the greater the pore size and particle size also.

5. Physical parameters determination

The refractive index of an aerogel is directly proportional to its density. Thus, the lower its density, the smaller its refractive index. The optical properties of aerogels are dependent on their pore size distribution, particle density and surface roughness. When the pore size is large, Rayleigh scattering will be greater, and hence the aerogels are seen as opaque. The particles in the aerogels will act as Rayleigh scattering centers and the scattering intensity is determined according to eqn (7),

$$I = \frac{8\pi^4 r^6 n^2 - 1}{d^2 \lambda^4 n^2 + 2}\left(1 + \cos^2\theta\right) \quad (7)$$

where θ is the scattering angle, r is the pore size, λ is the wavelength of light, n is the refractive index and d is the distance between the particle and the detector. Thus, as the r value increases, the scattering intensity increases, thereby decreasing the optical transmission.[87] Aerogels containing more alkyl groups will show more surface silylation, resulting in a greater spring back effect, which leads to a larger pore size. Thus, as the pore size increases, it will promote light scattering, leading to the formation of opaque aerogels. Therefore, aerogels based on trialkyl silanes will have larger pores and are generally less transparent compared to monoalkyl silanes such as MTMS.[54] The optical transmittance can be controlled by washing the gels with NH_4F and modifying them with silylating agents in the presence of an aprotic solvent.[82]

Contact angle measurements are conducted to determine the hydrophobicity of aerogels. It has been found that as the length of the alkyl chain increases, the contact angle also increases. The excess organic groups help in improving the degree of hydrophobicity together with an increase in the compressive strength and toughness of the aerogels. Better hydrophobicity values were also reported by the incorporation of R–(OCH_3), where surface methyl groups help in improving the hydrophobicity. The % water absorption is more for MTMS-based aerogels as they have less organic groups compared to di- and tri-alkyl chain silylating agents. If 'n' is high, according to eqn (5), the number of Si–R groups that replace –H will be high, and hence the hydrophobicity will also be high. A reduction in residual –OH groups can also help to improve the hydrophobicity. It is clear from the FTIR spectra that with an increase in the number of alkyl groups, the C–H absorption intensity is high and the –OH absorption peak is reduced.[54] Information about the various chemical bonds can be obtained from the FTIR spectra of the aerogels. Table II highlights the important peaks observed in the FTIR spectra of silica aerogels.

With an increase in the alkyl chain length, the porosity is found to increase. The porosity and thermal conductivity exhibit an inverse relationship. As the porosity increases, the heat conducted by the solid network will be low given that a large porosity means less solid network, and hence a decrease in thermal conductivity. Specifically, the thermal conductivity increases with an increase in the bulk density of the aerogels. The thermal conductivity of MTMS and HMDZ aerogel is reported to be 0.164 and 0.091 W m^{-1} K^{-1}, respectively. Very low thermal conductivity (0.009–0.0002 W m^{-1} K^{-1}) hydrophobic aerogels from wheat husk ash were reported by Liu *et al.* in 2016. TMCS was used as the hydrophobic agent,[33] which together with PMMA could further improve the mechanical and structural properties of the aerogels.[64]

The hydrophobicity of the aerogels are retained up to 325 °C, after which the Si–CH_3 groups get oxidized to Si–OH, which is established by the sharp exothermic peak in DTA. The weight will be greater with an increase in the alkyl chain length due to the presence of more organic groups.[54]

In a recent study, modelling and optimization of the silica aerogel synthetic parameters were explored, where the response surface methodology employing the central composite design (CCD) method was chosen for modelling. The minimum density (0.078 g cm^{-3}) aerogel was obtained under the constraints of 4.12 g L^{-1} silica concentration, 14.46 mL acid, and 10.39 mL TMCS. Furthermore, the material had a surface area of 780 m^2 g^{-1} under these conditions.[88]

For cylindrical aerogel monoliths, their volume is calculated from the diameter and height of the aerogel and mass using a microbalance manually. The bulk density (ρ_b) is measured using the known volume and mass. To calculate the refractive index, thew Clausius–Mossotti formula is used as follows:

$$n = \frac{3}{2}\frac{\rho}{\rho_S}\frac{{n_S}^2 - 1}{{n_S}^2 + 2} = 1 + 0.19\rho \quad (8)$$

where n and n_s are the refractive indices, and ρ and ρ_s are the density of the aerogel and silica, respectively. Considering that n_s and ρ_s for silica are known to be 1.46 and 2.2 g cm^{-3}, respectively, $n = 1 + 0.19\rho$ can be obtained.[54]

The porosity and pore diameter of the aerogel can be determined from the pore volume values, both of which are calculated using the following formulas:[21,41]

$$\text{Pore volume}\left(V_{\text{pore}}\right) = \left(\frac{1}{\rho_b} - \frac{1}{\rho_s}\right) \quad (9)$$

$$\text{Pore diameter}\left(D_{\text{pore}}\right) = \frac{4V_{\text{pore}}}{S_{\text{BET}}} \quad (10)$$

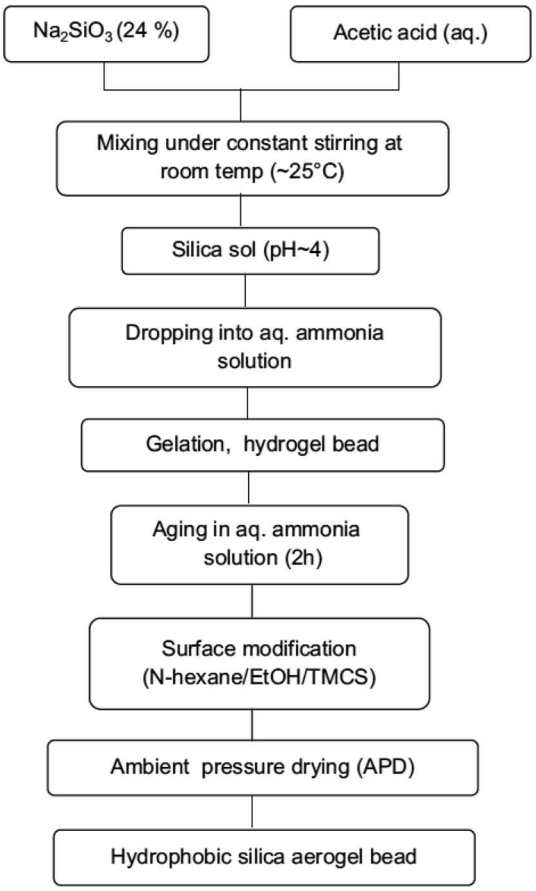

Fig. 6 Flow chart showing the preparation of silica aerogel beads.[43]

where S_{BET} is the specific surface area.[53]

$$\text{Porosity}(\%) = \left(1 - \frac{\rho_b}{\rho_s}\right)100 \quad (11)$$

where ρ_s is the skeletal density of the silica aerogel measured using a helium picnometer.[43]

Contact angle (θ) measurements will give the hydrophobic nature of the aerogel using the formula

$$\tan \theta/2 = \left(\frac{2I}{W}\right) \quad (12)$$

where I is the height of the water droplet and W is the base width of droplet touching the aerogel surface.

The thermal conductivity of the aerogel can be measured using a C-T meter according to the following equation:

$$\text{Thermal conductivity } (k): \Delta T = I^2 R/L4\pi k[\ln(t) + C] \quad (13)$$

where 'R' is the heater resistance (Ω), 'I' is the current flowing through the probe wire (A), 'L' is the heater length in metres, 'k' is the thermal conductivity (W m^{-1} K^{-1}) of the aerogel sample, 't' is the pulse time in seconds and 'C' is the integration constant.[21]

6. Aerogel powders and beads

Similar to aerogel monoliths, aerogel powders with a density as low as 0.05 g cm^{-3} and surface area 783 m^2 g^{-1} were prepared through fluidized bed drying. The prepared powders were super hydrophobic with a contact angle of 150°.[17,18] Thereafter, the fluidization technique was extensively used for the preparation of aerogels in granular and powder forms.[68] Spray drying can

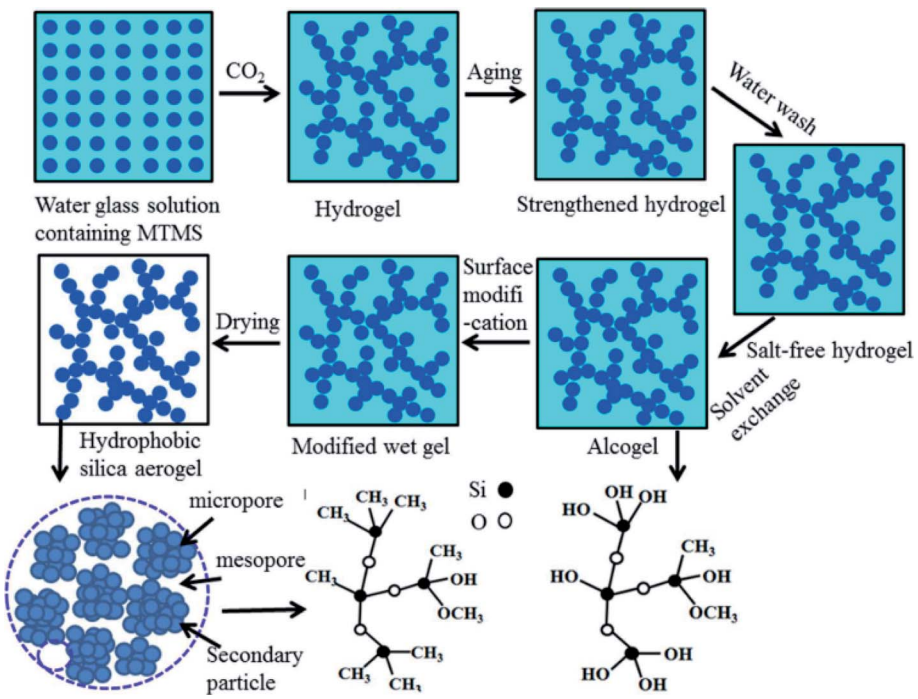

Fig. 7 Schematic route for the development of aerogels using CO_2 as a gelation agent.[81]

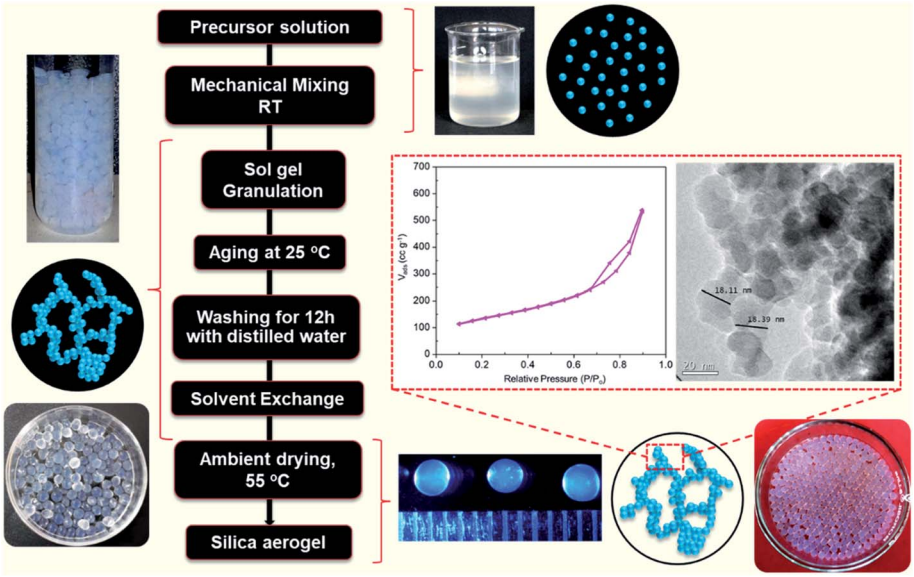

Fig. 8 Flow chart for the preparation of translucent aerogels.[60,91]

produce aerogel powders having a surface area of 870 $m^2 g^{-1}$.[75] To reduce the synthesis time and amount of modifier, mechanical crushing and filtration were used to produce super hydrophobic (WCA ~162°) aerogel powders by Pan *et al.* in 2017.[83] Quasi-solvent-exchange-free ambient pressure drying was also tested to produce silica aerogels, where the fabrication time was reduced to 2 h using this method.[89]

Yeo *et al.* synthesized aerogel granules with an average diameter of 1 mm and thermal conductivity of 0.01 W m^{-1} K^{-1} and 95% porosity. The granules were formed *via* the dropwise addition of silica sol to a chemical bath having hexane, lanolin dehydrate emulsifier and pyridine catalyst. The gels were modified with TMCS to obtain the final aerogel product. By carefully modifying the drying conditions, desired properties such as high surface area and low density were obtained.[74] Transparent silica aerogel beads with a low density and high surface area, pore volume and pore size were prepared by P. B. Sarawade *et al.* in 2010 and 2012 (Fig. 2(iv and v), respectively).[42,43] A flow chart for the procedure is given in Fig. 6.

Sarawade and co-workers extensively studied the area of silica aerogel beads and analyzed the effect of various process parameters on the physico-chemical properties of the aerogels.[42,43,67,72,90] Transparent aerogels were prepared through single-step and two-step sol–gel reactions by Bangi *et al.* (Fig. 2(vi)).[44] To make the synthesis process cost effective, CO_2 gas was used as the gelation agent for the preparation of hydrophobic (154°) silica aerogels. MTMS acted as hydrolysis-condensation rate control agent (Fig. 7).[81] By modifying the process developed by Sarawade *et al.*, our group synthesized translucent silica aerogels and spheres with surface area values in the range of 305–474 $m^2 g^{-1}$. Isopropanol was used as the solvent exchange medium, and through ambient pressure drying, we obtained gels with a pore size of ~18 nm, as shown in Fig. 8.[60,91]

7. Applications

The emergence of silica aerogels has provided the possibility to solve a wide array of problems in high-tech science and engineering. They have found broad applications in the fields of thermal insulation, separation, coatings, catalysis, hypervelocity particle capture, radiation detectors, *etc.* (Fig. 9).[7,60,92–95] According to an initial economic analysis, the cost of the starting materials was found to be the major factor influencing the manufacturing cost of aerogels, which favors the use of the inexpensive sodium silicate precursors.

7.1 Sodium silicate aerogels as composites and hybrids

To overcome the mechanical fragility of aerogels, composites of silica aerogels were prepared by immersing glass wool in silica sol by Kim *et al.* in 2007.[76] Post treatment with TMCS followed by heat treatment at 230 °C led to the development of aerogel composites. The composites were used for making silica aerogel blankets with a thermal conductivity of 0.026 W m^{-1} K^{-1}. In 2015, L. Amirkhani *et al.* prepared silica aerogel-iron oxide nanocomposites and observed that with an increase in the iron oxide content, the density and surface area of the aerogels increased.[96] In another study, Fe_3O_4–SiO_2 nanocomposites were prepared to explore their super paramagnetic behaviour. The saturation magnetization values were 34.5, 18.2 and 8.3 emu g^{-1} for 90, 70 and 50 wt% Fe_3O_4/SiO_2 nanocomposites respectively. With an increase in SiO_2 content, the particle size of Fe_3O_4 slightly decreased.[97] TiO_2–SiO_2 oxide composites were used for the modification of polyester fabric as a UV shielding material with UPF values of around 50 in another study.[98]

The preparation of biocomposites was also attempted using sodium silicate. Cellulose silica composite aerogels were prepared by Arnaud Demilecamps *et al.*[94] The addition of sodium silicate to a cellulose–NaOH solution considerably

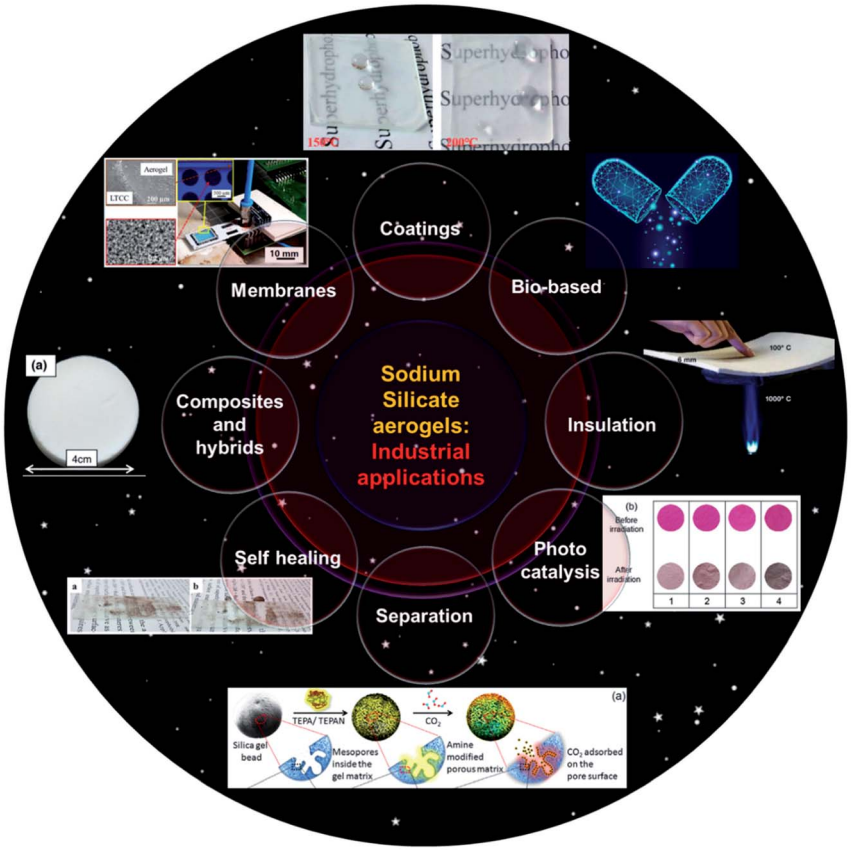

Fig. 9 Industrial applications of sodium silicate aerogels.[7,60,92–95]

decreased the gelation time. PEG–silica composites from rice husk char could produce porous silica with specific surface areas in the range of 709 to 936 $m^2\ g^{-1}$.[28]

Hybrid aerogel fibrous materials were prepared by blending water glass with nanofibrous polyester materials *via* electrospinning towards hydrophobic textiles. Due to the dual scale surface roughness of the hybrid, higher hydrophobicity and better adhesion strength were observed compared to pure polyester. Although no significant difference was observed for the water vapour permeability of polyester even after the incorporation of the aerogel, the air permeability improved with an increase in the aerogel content.[65]

7.2 Aerogels for coatings

The ambient pressure drying was further extended for thin film coatings by Cha *et al.* in 2007.[99] The coating was found to be continuous with a grain size of 20 nm and hydrophobicity was achieved by grafting trimethylchlorosilane (TMCS) on the surface. The heat treatment at 300 °C reduced the contact angle from 118° to 44°, rendering the nature from hydrophobic to hydrophilic.

7.3 Aerogels for bio-based applications

Microspheres of aerogels were prepared by an emulsion-gelation method with polysaccharide bases such as alginate, pectin and starch. The aerogels were studied for the release of the drug ketoprofen and benzoic acid. The drug loading varied depending on the aerogel structure and composition. The loading was 1.0×10^{-3} and 1.7×10^{-3} g m^{-2} for ketoprofen and benzoic acid, respectively, in the starch–silica microspheres.[62]

7.4 Aerogels for insulation

Aerogel materials offer significant potential towards improved energy efficiency through their use in high performance insulation boards. Table III shows the cost of different aerogels used

Table 3 Cost of aerogel per board foot (adapted from ref. 81)

Aerogel costs	
Material	Aerogel cost ($/board foot)
TMOS	7.91
TEOS	4.15
Sodium silicate	0.63
Resorcinol-formaldehyde (RF)	1.34
Phenol-formaldehyde (PF)	0.42
RF : PF (50 : 50)	0.89
Melamine-formaldehyde	1.14
Phenolic-furfural	0.73

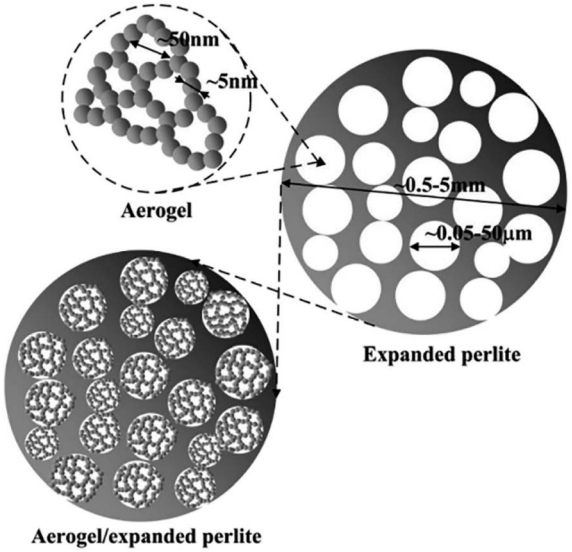

Fig. 10 Schematic diagram of the synthesis of AEP composites.[71]

for building insulation. The cost of the starting material is the major factor influencing the manufacture of insulation boards.[100] In addition to cost benefits, sodium silicate-based insulation boards have the added advantage of non-toxicity and are environmentally friendly.

The heat transfer mechanism of porous materials depends on five parameters, *i.e.*, solid, gaseous, radial, convective and coupling of solid and gaseous thermal conductivities, which are represented as λ_s, λ_g, λ_r, λ_c and $\lambda_{coupling}$, respectively. Aerogels have very low thermal conductivity (λ_{total}) owing to their low λ_s due to their complicated three-dimensional nanonetworks, low λ_g due to the Knudsen effect caused by their mesoporous nature and low λ_r due to their transparent nature in the infrared spectral range. The factor λ_c is neglected for a pore size less than 1 mm at ambient pressure.[71,101] With an increase in temperature, the thermal conductivity of aerogels increase.[45]

Aerogel-expanded perlite (AEP) composites were studied by different researchers. In the work done by Wang *et al.* in 2011, AEP composites were produced with a thermal conductivity of 0.077 W m^{-1} K^{-1}.[102] Later in 2017, Jia *et al.* prepared AEP composites by absorbing the silica hydrosol in to the porous structure of expanded perlite (EP) (Fig. 10). EP had a very low surface area of up to 3.3 m^2 g^{-1} and thermal conductivity of 0.044–0.047 W m^{-1} K^{-1}. Compared to EP, for AEP composites, the BET surface area increased by 50–150 times (up to 250 m^2 g^{-1}) and the thermal conductivity decreased by 14.7–31.8% (0.030–0.038 W m^{-1} K^{-1}).[71]

Encapsulating silica aerogel particles with flexible polymers improves their mechanical properties. In a recent study done by Halim *et al.* in 2018, hydrophobic silica aerogel particles were coated with polyvinyl alcohol *via* the fluidized bed coating method. The thermal conductivity of the materials decreased by 14% from 0.041 W m^{-1} K^{-1} to 0.035 W m^{-1} K^{-1} with PVA coating, which was explained by the decrease in thermal diffusivity by 16% after coating.[46] When the thermal diffusivity was

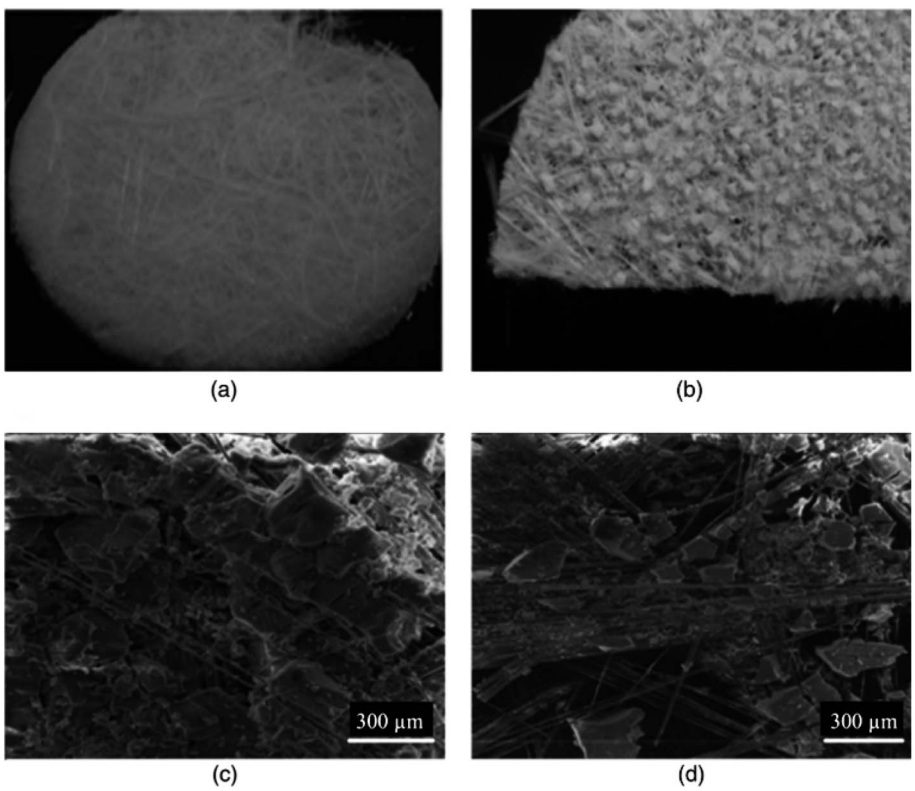

Fig. 11 Picture and SEM image of aerogel–glass fiber composites aged under (a and c) acidic and (b and d) basic conditions.[63]

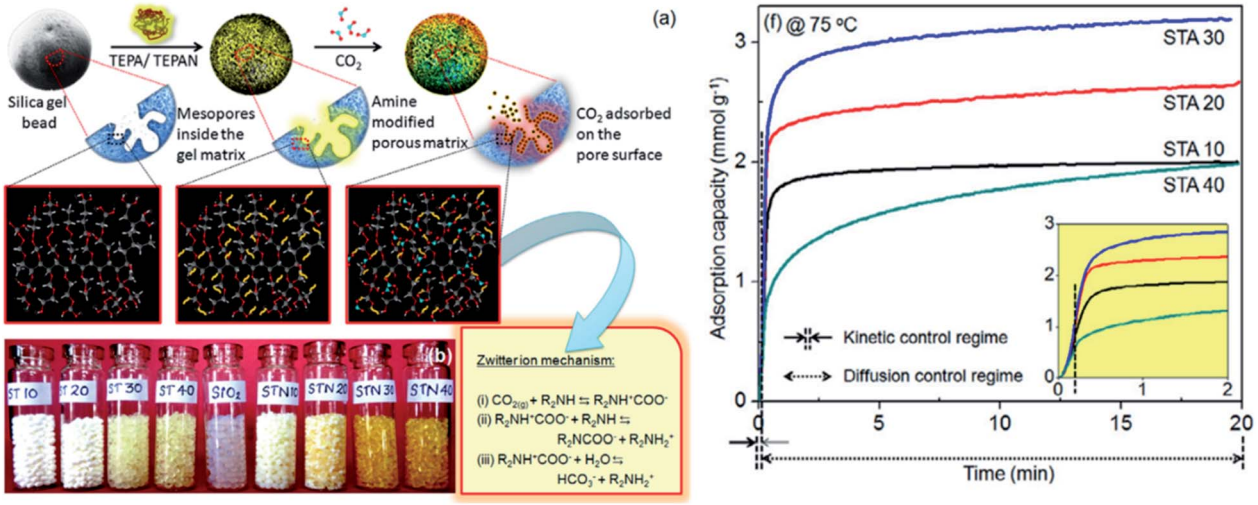

Fig. 12 (a) Reaction scheme for the adsorption of CO_2 on amine-modified silica aerogel and (b) CO_2 adsorption capacity at 75 °C.[60]

low, the heat transfer from the hot end to the inside pores of the aerogel can be reduced further, lowering the thermal conductivity.

Composites of unsaturated polyester (UP) resin and silica aerogel were prepared by Halim *et al.* in 2018 by mixing 70 vol% UP resin with 30 vol% silica aerogel. The prepared aerogels had a bulk density of 0.08 g cm^{-3}, surface area of 773 m^2 g^{-1} and pore size in the range of 11–18 nm. For the UP/SA composites, the density increased to 1.21 g cm^{-3}. The addition of 30 vol% SA decreased the thermal conductivity of the composite by 55% from 0.46 W m^{-1} K^{-1} to 0.2 W m^{-1} K^{-1}. It was suggested that the complex open pores of SA restricted the heat diffusion and heat transfer through the UP matrix.[27]

Kow *et al.* extracted silica from bamboo leaves and used it for the preparation of sodium silicate, and subsequently the synthesis of aerogels. The activated carbon obtained from the same source was used to opacify the aerogel and reduce the thermal conductivity. The thermal conductivity was determined to be 0.0324 W m^{-1} K^{-1} for the bamboo leaf aerogel.[34] Aerogels from recycled coal gangue could produce the thermal insulation of 26.5 × 10^{-3} W m^{-1} K^{-1}.[84]

Silica aerogel–glass fiber composites were studied for fire shielding of steel frame structures by Motahari *et al.* in 2015. Surface modification was carried out using TMCS/*n*-hexane/methanol solution having a volume ratio of 3/30/1 for 24 h. The optimum fire resistance was obtained for the sample with 89.7% porosity prepared at pH 4 with an aging time of 24 h. The aerogels prepared under basic conditions poorly covered the glass fibers. The fire resistance increased with an increase in % porosity and decrease in shrinkage. When the shrinkage was more, cracks developed in the aerogel and the hot gases could pass through the crazes and directly hit the glass fibers, reducing the fire retardance (Fig. 11).[63] Aerogel microgranules were used as fillers in PET nanofibers to improve the dyeing rate and thermal insulation of the composites. A decreasing heat transfer trend from 21% to 8.3% was observed for the pure nanofibers *vs.* 4 wt% aerogel-PET composites.[65] Fiber-reinforced silica aerogel monoliths functionalised with MTES and TMCS could produce composites with thermal conductivities in the range of 0.021–0.031 W m^{-1} K^{-1} and the average modulus of 323–535 kPa.[69]

Recently, thermal insulating aerogel powders modified with TMCS and HMDS with a thermal conductivity of 0.022 W m^{-1} K^{-1} were reported by Pooter *et al.* in 2018.[70]

Technically and economically viable forms of silica aerogels have been successfully commercialized by Aspen Aerogels, Inc. USA for over a decade. They offer high performance aerogel insulation blankets comprised of synthetic amorphous silica (SAS) over a wide range of products such as Pyrogel®, Cryogel® and Spaceloft® aerogel blanket insulation. The process integrates aerogels into a fiber-batting reinforcement to form flexible, resilient and durable blankets, which have applications in the industrial and building insulation markets.[95]

7.5 Aerogels for separation processes

The absorption of organic liquids with super hydrophobic aerogels (water contact angle > 161°) was studied by He *et al.* in 2015.[56] The aerogels were modified with TMCS to make them hydrophobic. The TMCS to pore water molar ratio was fixed at 0.0233 to avoid the excess use of TMCS. *N*,*N*-Dimethylformamide (DMF) was added as a drying control chemical additive before the hydrolysis of the sol. Excess DMF made the condensation rate higher and there was no improvement in properties. When the molar ratio of Si to DMF was 2.23, the obtained aerogels had better properties. Specifically, 1 cm^3 of aerogel could absorb around 0.9 mL of organic liquids *n*-hexane, ethanol and gasoline.

Hydrophobic silica aerogels were prepared from industrial micro silica *via* modification with TMCS and their oil adsorbing properties were studied by Fei Shi *et al.* in 2013. The aerogels prepared with an NaOH/microsilica weight ratio of $R = 1$ achieved an adsorption rate of 1105% after 60 min.[77]

Pouretedal *et al.* studied the adsorption of metal ions by silica aerogels and the optimum was noted to be 90.1, 181.8,

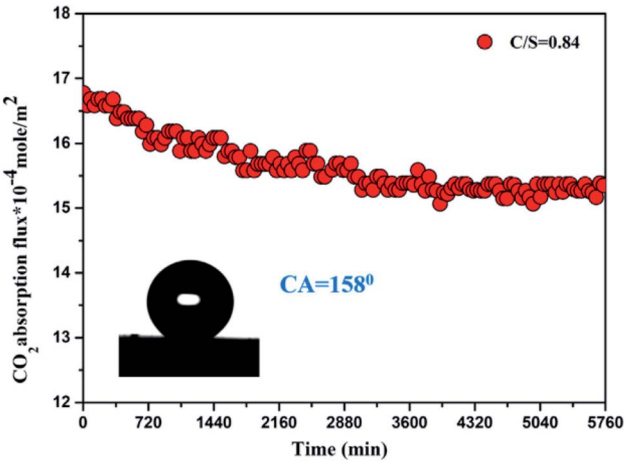

Fig. 13 CO_2 absorption flux of silica aerogel membrane.[86]

and 250.0 mg g^{-1} for Cu^{2+}, Cd^{2+}, and Pb^{2+} ions, respectively. The adsorption capacity improved with an increase in pH, contact time and adsorbent dose and decreased with an increase in initial concentration.[61]

Hydrophobic silica aerogels *via* the co-precursor method employing silylating agents TMCS, TEOS and HMDS were prepared for oil adsorption studies in another study. The silica aerogels modified with HMDS had the highest surface area of 936 m^2 g^{-1} and could remove 96% oil from oily waste water.[78]

The adsorption of naphthalene from aqueous solution was evaluated by adopting the central composite design approach, which indicated that contact time and adsorbent dose were important parameters. A second-order model was proposed for adsorption. The hydrophobic aerogel could adsorb around 25 mg L^{-1} adsorbate at the optimum conditions of 120 min, 4 pH and 4 g L^{-1} adsorbent dose.[80]

In one of our studies, amine-modified silica aerogels were used for CO_2 adsorption studies at different temperatures with a maximum adsorption capacity of 3.26 mmol g^{-1} at 75 °C. CO_2 reacts with amines following a zwitterion mechanism. The colour of the aerogel turned from translucent to yellow upon amine functionalization (Fig. 12). It was observed that primary amines improved the adsorption capacity and secondary amines enhanced the kinetics of adsorption.[60]

Lin *et al.* used silica aerogel membranes for CO_2 capture, that exhibited a high CO_2 absorption flux of 1.5 mmol m^{-2} s^{-1}. The high contact angle (158°) prevented membrane swelling during absorption (Fig. 13).[86]

7.6 Aerogels for photocatalysis

The photocatalytic activity of hydrophobic TiO_2–SiO_2 aerogels has been explored by different research groups.[73,103] The catalytic performance is influenced by the hydrophobicity, porous and amorphous nature of the aerogels. To improve the photocatalytic activity, W-doped TiO_2 was used for the preparation of SiO_2 aerogel/W_xTiO_2 composites. With an increase in SiO_2 content, the specific surface area and pore volume of the composites improved. The sample 0.9STW-1:3 exhibited 97% removal efficiency for Rhodamine B from water.[93]

7.7 Other applications

Silica aerogel membranes were designed with low thermal conductivity and high air conductance for miniaturized thermomolecular air pump applications (Fig. 2(vii)). The optimum pumping performance was found for the membranes having a density of 0.062 g cm^{-3} and pore size of 142 nm.[7]

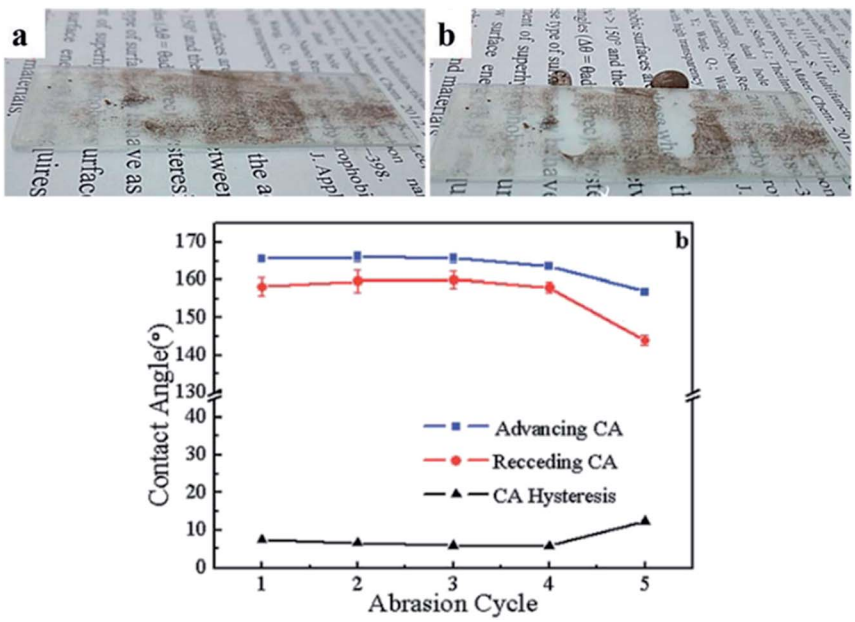

Fig. 14 Optical images of (a) dusty surface of aerogel coating, (b) self-cleaned surface and (c) effect of sand paper abrasion cycle on contact angle.[92]

Table 4 Summary of sodium silicate-derived aerogels for various industrial applications

Material	Application	Property utilised	Remarks	Ref.
MPTMS modified silica aerogel	Adsorbent for Cu^{2+}, Cd^{2+}, and Pb^{2+} ions	Surface area	The optimum adsorption values are found as 90.1, 181.8, and 250.0 mg g^{-1}, respectively, for Cu^{2+}, Cd^{2+}, and Pb^{2+} ions; contact time = 30 min, adsorbent dose = 0.05 g and pH = 6 for Cd^{2+} and Pb^{2+} ions, adsorbent dose = 0.1 g and pH = 4 for Cu^{2+} ions	Pouretedal 2012 (ref. 61)
TEPA/APTMS modified silica aerogel	CO_2 adsorbent	Surface area/ porosity	CO_2 adsorption capacity of 3.26 mmol g^{-1} at 75 °C, 1 atm pressure	Minju 2017 (ref. 60)
Polysaccharide-based aerogel microspheres	Oral drug delivery	Specific surface area and surface chemistry	An amorphous drug-loaded delivery system with loadings in the range of 11–24 wt%. Specific loading capacity up to 1.54×10^{-4} g m^{-2} for ketoprofen and 2.38×10^{-4} g m^{-2} for benzoic acid was obtained	Garcia 2015 (ref. 62)
Silica aerogel–PVA core–shell	Thermal insulation	Thermal conductivity	The thermal conductivity of the core shell structure (0.035 W m^{-1} K^{-1}) was lower than that of silica aerogel (0.041 W m^{-1} K^{-1}) owing to good thermal insulation and very thin coating of PVA. The PVA shell also remarkably improved the thermal stability	Halim 2018 (ref. 46)
Silica aerogel–Glass fiber composites	Fire shield for steel frame structures	Porosity	The composites made at pH 4 show considerably higher fire resistance (28–42 min.) compared to those made at pH 8 (11–23 min). The highest fire resistance was obtained for samples with 89.7% porosity and the lowest fire resistance for samples with 58.2% porosity	Motahari 2015 (ref. 63)
Super hydrophobic hybrid aerogel powder	Water transport at microscale level	Hydrophobicity	Hybrid aerogel powder with high lipophilic/ hydrophilic ratios were achieved, with tapping densities as low as 0.120 g cm^{-3} and contact angle up to 152°	Julio 2014 (ref. 57)
Silica aerogel powder	Thermal insulation	Pore size/pore volume	Aerogels modified with HMDSO achieved thermal conductivity as low as 0.022 W m^{-1} K^{-1}	Pooter 2018 (ref. 70)
Aerogel/expanded perlite (AEP) composite	Thermal insulation	Mesopore volume, surface area, thermal conductivity	The mesoporous volumes and BET specific surface areas of AEP (0.58–1.06 cm^3 g^{-1} and 139–250 m^2 g^{-1}) were about 100–280 times and 50–150 times that of expanded perlite EP (3.78 E^{-3}–8.32×10^{-3} and 1.62–3.31 m^2 g^{-1}), respectively. The thermal conductivities of AEP (0.03–0.038 W m^{-1} K^{-1}) decreased by 14.7–31.8% compared to that of EP (0.044–0.047 W m^{-1} K^{-1})	Jia 2018 (ref. 71)
TiO_2–SiO_2 aerogel composites	Photo catalysis	Surface area, super ior textural properties, hydrophobicity	The as-synthesized TiO_2–SiO_2 aerogel composite was hydrophobic and exhibited the highest activity toward decolorization of methylene blue. Calcination tailored the property from hydrophobic to hydrophilic and the formed samples possessed lower activities	Kim 2013 (ref. 73)
Super hydrophobic SiO_2 surface	Scratch & heat resistance, self-cleaning	Hydrophobicity	The super hydrophobic (water contact angle and sliding angle 169.80° and 4°) coatings maintained water repellency under 350 °C for 4 h and durable super- hydrophobicity for 6 months at ambient conditions and excellent thermal and mechanical stabilities (abrasion resistance under (∼2178 Pa pressure applied)	Zhao 2018 (ref. 92)
Silica aerogel membranes	Membranes for miniaturized motionless gas pumps	Density, pore size, surface modification	Optimal pumping performance was found for devices with integrated membranes with low-density (0.062 g cm^{-3}) and an average pore size of 142 nm. The membranes gave an air flow rate density of 3.85 sccm cm^{-2} at an operating temperature of 400 °C	Zhao 2015 (ref. 7)
Silica aerogel coated on macroporous Al_2O_3 membrane supports	Membranes for CO_2 absorption	Hydrophobicity	A stable CO_2 absorption flux of 1.5 mmol m^{-2} s^{-1} was observed and the membranes could be used continuously for at least 4 days	Lin 2019 (ref. 86)
TiO_2–SiO_2 oxide composites	Barrier properties against UV radiation of textile fabrics	Surface area	Modification of polyester woven and nonwoven fabric with oxide composites increased the UPF values to above 50	Stefanska 2012 (ref. 98)
Hydrophobic silica aerogel	Oil adsorption	Density, pore volume, hydrophobicity	Silica aerogel with NaOH/microsilica weight ratio R = 1.0 had the highest pore volume and excellent adsorption for engine oil. The saturated oil adsorption rate was 1105% after 60 minutes	Shi 2013 (ref. 77)

Table 4 (*Contd.*)

Material	Application	Property utilised	Remarks	Ref.
Hydrophobic silica aerogel	Oil adsorption	Surface area, contact angle, pore volume	Silica aerogel prepared from HMDS showed maximum oil removal of 96% and 90% from saline and non-saline oily wastewater, respectively	Sorour 2016 (ref. 78)
Expanded perlite (EP) modified by aerogel	Thermal insulation	Thermal conductivity, pore size	Aerogel-modified EP board had a lower thermal conductivity (0.077 W m^{-1} K^{-1}) than unmodified EP board (0.083 W m^{-1} K^{-1})	Wang 2011 (ref. 102)
Silica aerogel	Thermal insulation	Thermal conductivity, bulk density	The final aerogel material presents a good thermal insulation property of 26.5 × 10^{-3} W m^{-1} K^{-1}	Zhu 2016 (ref. 84)
SiO_2/TiO_2 aerogel composites	Photo catalytic activity	Surface area, pore size	The binary aerogel composite exhibited significant photocatalytic efficiency, the decolorizing efficiency for methyl orange reached 84.9% after 210 min UV light irradiation	Xu 2016 (ref. 103)
Silica aerogel	Naphthalene adsorption	Surface area, pore volume, density, hydrophobicity	The optimum adsorption parameters obtained through central composite design (CCD) approach was time 120 min, pH = 4 and amount of adsorbent 4 g L^{-1} with an experimental adsorption capacity of 24.68 mg L^{-1} and a predicted value of 24.9 mg L^{-1}	Yaqubzadeh 2016 (ref. 80)

Super hydrophobic (WCA ~169°) semi-transparent silica aerogels having multifunctional properties such as scratch and heat resistance and self-cleaning were proposed by Zhao *et al.* in 2018. The nanoparticles after silylation were wrapped with PDMS to make them super hydrophobic. The coatings remained super hydrophobic even after four rounds of abrasion with sand paper under more than 2000 Pa (Fig. 14).[92]

The applications of different aerogels are summarized in Table IV.

8. Summary and outlook

During the past few years, numerous aerogel products have penetrated the commercial market. The starting material used plays an important role in deciding the final properties and total production cost. Sodium silicate-based aerogels have found wide applications owing to their cheap raw material cost. The ambient pressure dried aerogels provide the same properties as their analogues, which are organosilane-derived and super critically dried aerogels. Tailoring the important parameters such as molar ratio, sol pH, gelation time, aging, washing, solvent exchange, and silylating agents used can alter the physico-chemical characteristics of aerogels, offering distinct properties depending upon the specific applications. The ambient pressure drying method used can make the industrial production more economical. Also, silica aerogels have some added advantages such as non-toxicity and environmentally friendly nature compared to the other organic precursor-derived aerogels in the market. Considering that sol–gel derived silica can be cast into any shape and size at room temperature, they serve as a perfect host for organic molecules, polymers and fibers, and therefore can find more advanced applications such as insulation, membrane separation, sensing and other niche market areas.

Conflicts of interest

There are no conflicts of interest to declare.

References

1 T. E. of E. Britannica, n.d.
2 R. K. Iler, *The Chemistry of Silica: Solubility, Polymerization, Colloid and Surface Properties and Biochemistry*, John Wiley & Sons Inc., 1979.
3 M. M. Koebel and S. Zhao, *Empa*, 2013, 1–12.
4 C. J. Brinker and G. W. Scherer, *Sol-gel science: The physics and chemistry of sol-gel processing*, Academic Press, INC., 1990, pp. 1–908.
5 B. N. Nair, T. Yamaguchi, T. Okubo, H. Suematsu, K. Keizer and S. I. Nakao, *J. Membr. Sci.*, 1997, **135**, 237.
6 B. N. Nair, K. Keizer, T. Okubo and S. I. Nakao, *Adv. Mater.*, 1998, **10**, 249.
7 S. Zhao, B. Jiang, T. Maeder, P. Muralt, N. Kim, S. K. Matam, E. Jeong, Y.-L. Han and M. M. Koebel, *ACS Appl. Mater. Interfaces*, 2015, **7**, 18803.
8 J. L. Gurav, I.-K. Jung, H.-H. Park, E. S. Kang and D. Y. Nadargi, *J. Nanomater.*, 2010, **2010**, 1.
9 M. A. Aegerter, N. Leventis and M. M. Koebel, *Advances in Sol-Gel Derived Materials and Technologies*, Springer, 2011.
10 M. J. Muñoz-Aguado and M. Gregorkiewitz, *J. Colloid Interface Sci.*, 1997, **185**, 459.
11 B. L. Newalkar and S. Komarneni, *J. Sol-Gel Sci. Technol.*, 2000, **18**, 191.
12 B. N. Nair, W. J. Elferink, K. Keizer and H. Verweij, *J. Colloid Interface Sci.*, 1996, **178**, 565.
13 S. S. Kistler, *Nature*, 1931, **127**, 741.
14 S. S. Kistler, *J. Phys. Chem.*, 1932, **36**, 52.
15 D. M. Smith, R. Deshpande and C. J. Brinker, *Mater. Res. Soc. Symp. Proc.*, 1992, **271**, 567.

16 P. M. Shewale, A. V. Rao and A. P. Rao, *Appl. Surf. Sci.*, 2008, **254**, 6902.
17 S. D. Bhagat, K. T. Park, Y. H. Kim, J. S. Kim and J. H. Han, *Solid State Sci.*, 2008, **10**, 1113.
18 S. D. Bhagat, Y. H. Kim, K. H. Suh, Y. S. Ahn, J. G. Yeo and J. H. Han, *Microporous Mesoporous Mater.*, 2008, **112**, 504.
19 U. K. H. Bangi, A. V. Rao and A. P. Rao, *Sci. Technol. Adv. Mater.*, 2008, **9**, 1–10.
20 S. W. Hwang, T. Y. Kim and S. H. Hyun, *J. Colloid Interface Sci.*, 2008, **322**, 224.
21 A. P. Rao, A. V. Rao and J. L. Gurav, *J. Porous Mater.*, 2008, **15**, 507.
22 K. Sinkó, N. Hüsing, G. Goerigk and H. Peterlik, *Langmuir*, 2008, **24**, 949.
23 F. Schwertfeger, D. Frank and M. Schmidt, *J. Non-Cryst. Solids*, 1998, **225**, 24.
24 Z. S. Zhou, C. S. Li, J. Z. Jin and X. H. He, *J. Non-Cryst. Solids*, 2007, **353**, 2774.
25 T. Li and T. Wang, *Mater. Chem. Phys.*, 2008, **112**, 398.
26 J. P. Nayak and J. Bera, *Trans. Indian Ceram. Soc.*, 2009, **68**, 91.
27 Z. A. A. Halim, M. A. M. Yajid, M. H. Idris and H. Hamdan, *J. Macromol. Sci., Part B: Phys.*, 2018, **57**, 479.
28 D. Li and X. Zhu, *Mater. Lett.*, 2011, **65**, 1528.
29 B. Karakuzu, T. M. Temel, S. Yucel, P. Terzioğlu and Y. Elalmış, *Sigma J. Eng. Nat. Sci.*, 2016, **34**, 175.
30 C. Sheng, Y. Shu-wen, L. Ben-lan, S. Xiao-dong and G. Danming, *RSC Adv.*, 2015, 1.
31 A. Tadjarodi, M. Haghverdi and V. Mohammadi, *Mater. Res. Bull.*, 2012, **47**, 2584.
32 T. M. Temel, B. K. İkizler, P. Terzioğlu, S. Yücel and Y. B. Elalmış, *J. Sol-Gel Sci. Technol.*, 2017, **84**, 51.
33 S. W. Liu, Q. Wei, S. P. Cui, Z. R. Nie, M. H. Du and Q. Y. Li, *J. Sol-Gel Sci. Technol.*, 2016, **78**, 60.
34 K. W. Kow, R. Yusoff, A. R. A. Aziz and E. C. Abdullah, *Trans. Indian Ceram. Soc.*, 2016, **75**, 175.
35 N. Nazriati, H. Setyawan, S. Affandi, M. Yuwana and S. Winardi, *J. Non-Cryst. Solids*, 2014, **400**, 6.
36 F. Shi, J. X. Liu, K. Song and Z. Y. Wang, *J. Non-Cryst. Solids*, 2010, **356**, 2241.
37 Y. Cheng, M. Xia, F. Luo, N. Li, C. Guo and C. Wei, *Colloid. Surface. Physicochem. Eng. Aspect.*, 2016, **490**, 200.
38 Y. R. Lee, J. T. Soe, S. Zhang, J. W. Ahn, M. B. Park and W. S. Ahn, *Chem. Eng. J.*, 2017, **317**, 821.
39 T. M. A. Khan, A. Khan and P. B. Sarawade, *AIP Conf. Proc.*, 2018, **1953**, 030274-1–030274-5.
40 H. Y. Nah, V. G. Parale, H. N. R. Jung, K. Y. Lee, C. H. Lim, Y. S. Ku and H. H. Park, *J. Sol-Gel Sci. Technol.*, 2018, **85**, 302.
41 S. He, Z. Li, X. Shi, H. Yang, L. Gong and X. Cheng, *Adv. Powder Technol.*, 2015, **26**, 537.
42 P. B. Sarawade, D. V. Quang, A. Hilonga, S. J. Jeon and H. T. Kim, *Mater. Lett.*, 2012, **81**, 37.
43 P. B. Sarawade, J. K. Kim, A. Hilonga and H. T. Kim, *Solid State Sci.*, 2010, **12**, 911.
44 U. K. H. Bangi, I. K. Jung, C. S. Park, S. Baek and H. H. Park, *Solid State Sci.*, 2013, **18**, 50.
45 G. Liu, B. Zhou, X. Ni, J. Shen, G. Wu, A. Du and G. Zu, *J. Sol-Gel Sci. Technol.*, 2012, **62**, 126.
46 Z. A. Abdul Halim, M. A. Mat Yajid, M. H. Idris and H. Hamdan, *Mater. Chem. Phys.*, 2018, **215**, 269.
47 Z. Shao, F. Luo, X. Cheng and Y. Zhang, *Mater. Chem. Phys.*, 2013, **141**, 570.
48 A. V. Rao, A. P. Rao and M. M. Kulkarni, *J. Non-Cryst. Solids*, 2004, **350**, 224.
49 P. B. Sarawade, J.-K. Kim, J.-K. Park and H.-K. Kim, *Aerosol Air Qual. Res.*, 2006, **6**, 93.
50 G. Geng, W. Bi, Y. Zhang and D. Sun, *Adv. Mater. Res.*, 2010, **148–149**, 1491.
51 B. Knoblich and T. Gerber, *J. Non-Cryst. Solids*, 2001, **283**, 109.
52 J. L. Gurav, A. V. Rao, A. P. Rao, D. Y. Nadargi and S. D. Bhagat, *J. Alloys Compd.*, 2009, **476**, 397.
53 S. Iswar, W. J. Malfait, S. Balog, F. Winnefeld, M. Lattuada and M. M. Koebel, *Microporous Mesoporous Mater.*, 2016, **241**, 293.
54 A. P. Rao, A. V. Rao and G. M. Pajonk, *Appl. Surf. Sci.*, 2007, **253**, 6032.
55 S. Lee, E. A. Lee, H. J. Hwang, J. W. Moon, I. S. Han and S. K. Woo, *Mater. Sci. Forum*, 2006, **510–511**, 910.
56 S. He, D. Huang, H. Bi, Z. Li, H. Yang and X. Cheng, *J. Non-Cryst. Solids*, 2015, **410**, 58.
57 M. D. F. Julio and L. M. Ilharco, *Microporous Mesoporous Mater.*, 2014, **199**, 29.
58 H. Y. Nah, V. G. Parale, K. Y. Lee, H. Choi, T. Kim, C. H. Lim, J. Y. Seo, Y. S. Ku, J. W. Park and H. H. Park, *J. Sol-Gel Sci. Technol.*, 2018, **87**, 319.
59 D. M. Smith, D. Stein, J. M. Anderson and W. Ackerman, *J. Non-Cryst. Solids*, 1995, **186**, 104.
60 N. Minju, B. N. Nair, A. Peer Mohamed and S. Ananthakumar, *Sep. Purif. Technol.*, 2017, **181**, 192.
61 H. R. Pouretedal and M. Kazemi, *Int. J. Ind. Chem.*, 2012, **3**, 1.
62 C. A. Garcia-Gonzalez, M. Jin, J. Gerth, C. Alvarez-Lorenzo and I. Smirnova, *Carbohydr. Polym.*, 2015, **117**, 797.
63 S. Motahari and A. Abolghasemi, *J. Mater. Civ. Eng.*, 2015, **27**, 04015008.
64 H. Ma, B. Wang, J. Han, Z. Lei and Y. Dawei, *Nanosci. Nanotechnol. Lett.*, 2016, **7**, 930.
65 Z. Mazrouei-Sebdani, A. Khoddami, H. Hadadzadeh, M. Zarrebini, A. Karimi and F. Shams-Ghahfarokhi, *Mater. Chem. Phys.*, 2016, **177**, 99.
66 Z. Azrouei-Sebdani, A. Khoddami, H. Hadadzadeh and M. Zarrebini, *RSC Adv.*, 2015, **5**, 12830–12842.
67 P. B. Sarawade, J. K. Kim, A. Hilonga, D. V. Quang and H. T. Kim, *Appl. Surf. Sci.*, 2011, **258**, 955.
68 G. M. Gao, D. R. Liu, H. F. Zou, L. C. Zou and S. C. Gan, *Powder Technol.*, 2010, **197**, 283.
69 Z. Shao, X. He, Z. Niu, T. Huang, X. Cheng and Y. Zhang, *Mater. Chem. Phys.*, 2015, **162**, 346.
70 S. De Pooter, S. Latré, F. Desplentere and D. Seveno, *J. Non-Cryst. Solids*, 2018, **499**, 217.
71 G. Jia, Z. Li, P. Liu and Q. Jing, *J. Non-Cryst. Solids*, 2018, **482**, 192.

72 P. B. Sarawade, J. K. Kim, A. Hilonga, D. V. Quang, S. J. Jeon and H. T. Kim, *J. Non-Cryst. Solids*, 2011, **357**, 2156.
73 Y. N. Kim, G. N. Shao, S. J. Jeon, S. M. Imran, P. B. Sarawade and H. T. Kim, *Chem. Eng. J.*, 2013, **231**, 502.
74 J. G. Yeo, J. M. Hong, C. H. Cho, S. D. Bhagat, Y. H. Kim and Y. S. Ahn, *Solid State Phenom.*, 2007, **124–126**, 675.
75 P. B. Sarawade, J. K. Kim, A. Hilonga and H. T. Kim, *Powder Technol.*, 2010, **197**, 288.
76 C. Y. Kim, J. K. Lee and B. I. Kim, *Mater. Sci. Forum*, 2007, **544–545**, 673.
77 F. Shi, J. Liu, X. Dong, Z. Zhang, P. Du, X. Wang and X. Zhang, *Key Eng. Mater.*, 2013, **531–532**, 103.
78 M. H. Sorour, H. A. Hani, G. A. Al-Bazedi and A. M. EL-Rafei, *J. Porous Mater.*, 2016, **23**, 1401.
79 Nazriati, H. Setyawan and S. Winardi, *AIP Conf. Proc.*, 2011, **1415**, 114.
80 A. R. Yaqubzadeh, A. Ahmadpour, T. R. Bastami and M. R. Hataminia, *J. Non-Cryst. Solids*, 2016, **447**, 307.
81 X. Wu, M. Fan, X. Shen, S. Cui and G. Tan, *Ceram. Int.*, 2018, **44**, 821.
82 A. Venkateswara Rao, V. V. Ganbavle, U. K. H. Bangi and S. L. Dhere, *J. Porous Mater.*, 2011, **18**, 751.
83 Y. Pan, S. He, X. Cheng, Z. Li, C. Li, Y. Huang and L. Gong, *J. Sol-Gel Sci. Technol.*, 2017, **82**, 594.
84 P. Zhu, M. Zheng, S. Zhao, J. Wu and H. Xu, *Adv. Mater. Sci. Eng.*, 2016, **2016**, 1.
85 U. K. H. Bangi, S. S. Pandit, D. B. Bagal and H.-H. Park, *Macromol. Symp.*, 2019, **387**, 1.
86 Y.-F. Lin, C.-R. Syu, K.-W. Huang and K.-Y. A. Lin, *Chem. Phys. Lett.*, 2019, **726**, 13.
87 P. M. Shewale, A. Venkateswara Rao, A. Parvathy Rao and S. D. Bhagat, *J. Sol-Gel Sci. Technol.*, 2009, **49**, 285.
88 S. S. Mirzaee, E. Salahi and A. Khanlarkhani, *Micro Nano Lett.*, 2018, **13**, 853.
89 J. Wang, Y. Zhang, Y. Wei and X. Zhang, *Microporous Mesoporous Mater.*, 2015, **218**, 192.
90 P. B. Sarawade, G. N. Shao, D. V. Quang and H. T. Kim, *Appl. Surf. Sci.*, 2013, **287**, 84.
91 N. Minju, P. Abhilash, B. N. Nair, A. P. Mohamed and S. Ananthakumar, *Chem. Eng. J.*, 2015, **269**, 335.
92 X. Zhao, J. Li, Q. Li, L. Qiao, L. Zhang, Z. Liu and C. Yang, *RSC Adv.*, 2018, **8**, 25008.
93 J. Liu, X. Wang, F. Shi, L. Yu, S. Liu, S. Hu and D. Liu, *Adv. Powder Technol.*, 2016, **27**, 1781.
94 A. Demilecamps, G. Reichenauer, A. Rigacci and T. Budtova, *Cellulose*, 2014, **21**, 2625.
95 Aspen aerogels, "About Aerogel and Aerogel Insulation," can be found under https://www.aerogel.com/resources/about-aerogel/, n.d.
96 L. Amirkhani, J. Moghaddas and H. Jafarizadeh, *Bulg. Chem. Commun.*, 2015, **47**, 82.
97 J. S. Lee, S. K. Hong, N. J. Hur, W. S. Seo and H. J. Hwang, *Mater. Lett.*, 2013, **112**, 153.
98 K. Siwińska-Stefańska, F. Ciesielczyk, A. Kołodziejczak-Radzimska, D. Paukszta, J. Sójka-Ledakowicz and T. Jesionowski, *Pigm. Resin Technol.*, 2012, **41**, 139.
99 Y. C. Cha, C. E. Kim, S. H. Lee, H. J. Hwang, J. W. Moon, I. S. Han and S. K. Woo, *Solid State Phenom.*, 2007, **124–126**, 671.
100 G. Carlson, D. Lewis, K. McKinley, J. Richardson and T. Tillotson, *J. Non-Cryst. Solids*, 1995, **186**, 372.
101 O. Lee, K. Lee, T. Jin and S. Young, *J. Non-Cryst. Solids*, 2002, **298**, 287.
102 Z. S. Wang, H. C. Tu, J. X. Gao, G. D. Qian, X. P. Fan and Z. Y. Wang, *Adv. Mater. Res.*, 2011, **250–253**, 507.
103 H. Xu, P. Zhu, L. Wang, Z. Jiang and S. Zhao, *J. Wuhan Univ. Technol. Mater. Sci. Ed.*, 2016, **31**, 80.